

**ION SCATTERING IN A SELF-CONSISTENT CYLINDRICAL PLASMA
SHEATH**

By

Shana S. Figueroa

A Thesis

Submitted to the Faculty

of the

WORCESTER POLYTECHNIC INSTITUTE

in partial fulfillment of the requirements for the

Degree of Master of Science

in

Mechanical Engineering

May 2006

APPROVED:

Dr. Nikolaos A. Gatsonis, Advisor
Professor, Mechanical Engineering Department

Dr. David Cooke, Co-Advisor
Air Force Research Lab, Hanscom AFB

Dr. William Durgin, Committee Member
Professor, Mechanical Engineering Department

Dr. John Blandino, Committee Member
Assistant Professor, Mechanical Engineering Department

Dr. Michael Demetriou, Committee Member
Associate Professor, Mechanical Engineering Department

Abstract

The Turning Point Method (TPM) for the evaluation of ion scattering in a sheath of a biased probe immersed in an unmagnetized plasma is reviewed. The TPM implemented originally in a computer program for spherical probes is expanded to include cylindrical probes as well as the evaluation of the turning angle of the charged particle (repelled or attracted) around the probe. TPM results have the potential to provide a standard against which to compare more complicated current collection simulations. TPM results are validated by comparing with Laframboise's earlier work for current collection in the Orbital Motion Limited regime. Calculations of the turning angle of a charged particle with specific energy and angular momentum revealed that higher plasma shielding limits the range of impact parameters that experience significant scattering, and that attracted particles entering tangent to the sheath experience increased scattering. The TPM results also show that there are significant changes in orbital trajectories between different space charges within the Orbital Motion Limited limit.

Acknowledgement

I'd like to thank everyone that helped me complete my thesis, including:

- Dr. David Cooke, my thesis co-advisor, for providing me with a thesis that I was able to pursue as part of my regular job at the Air Force Research Laboratory and guiding me to successful completion
- Dr. Nikolaos Gatsonis, my thesis advisor, for providing insights and approving of my thesis
- Kevin Ray, my supervisor at the Air Force Research Laboratory, for being very supportive of my career goals and allowing me the flexibility to attend classes at the WPI campus during work hours
- The United States Air Force for partially paying for my Master's degree and being generally pro-education, and displaying a surprising willingness to accommodate an officer's personal needs
- Chris St.Yves, my husband, for letting me put on some shoes and leave the kitchen to pursue an advanced degree, and only complaining a little bit when his dinner wasn't on the table by exactly 6pm each night
- My mother and father, for taking the time and effort to not drop me on my head when I was an infant. If it wasn't for their care, I am quite sure that I would not have been able to complete this thesis, or really do anything without the help of a permanent caregiver.

Table of Contents

Abstract	i
Acknowledgements	ii
Table of Contents	iii
List of Tables and Figures	v
Nomenclature	vii
1. Introduction	1
1.1. Plasma Probe Theory Review	1
1.1.1. Planar Langmuir Probes and the Planar Sheath.....	3
1.1.2. Spherical and Cylindrical Langmuir Probes	9
1.1.3. Plasma Analytical Models	11
1.1.3.1. Orbit Motion Limited	11
1.1.3.2. Effective-Potential Formulation	16
1.1.3.3. Turning Point Method	17
1.2. Review of the General Plasma Computer Model	18
1.3. Objectives and Methodology	21
2. Turning Point Method and Computer Program Structure	23
2.1. The Turning Point Method	23
2.1.1. The Vlasov Problem	23
2.1.2. The Poisson Problem	36
2.2. Turning Angle Calculations	37
2.3. Computational Applications of the Turning Point Method	40

2.3.1. Simultaneous Solution of the Vlasov and Poisson Problems Through Computational Means	40
2.3.2. Turning Angle Computations	45
3. Results and Validation	47
3.1. Cylindrical Probe Sheath Approximations	47
3.2. Turning Angle Approximations	50
4. Summary and Recommendations for Future Work	56
4.1. Summary of Work and Conclusions	56
4.2. Recommendations for Future Work	57
References	60

List of Tables and Figures

Figure 1.1. Thick- vs Thin-Sheathed Probes	4
Figure 1.2. Trajectory of a Positively Charged Particle Around a Negatively Charged Probe	10
Figure 1.3. Number Density n vs Potential ϕ (from <i>Laframboise, 1973</i>)	14
Figure 1.4. Current Density i vs Potential ϕ (from <i>Laframboise, 1973</i>)	15
Figure 1.5. The leap-frog method for calculating the force F while advancing V , and V while advancing x (from <i>Birdsall, 1985</i>)	19
Figure 2.1. The 4 Types of Orbits (from <i>Parker, 1976</i>)	26
Figure 2.2. Case A, B, and C in r, J^2 space (from <i>Parker, 1976</i>)	30
Figure 2.3. Attracted and Repelled Particle Trajectories	40
Figure 2.4. Graphical representation of the TurningPoint program flow	44
Figure 3.1. Electric Potential vs Radius from the Probe For Different Debye Lengths ..	47
Figure 3.2. Sheath Radius vs Probe Potential	48
Figure 3.3. Probe Current i vs Probe Potential ϕ_p for a Cylindrical Probe (from <i>Laframboise, 1966</i>)	49
Figure 3.4. Turning Angle vs Impact Parameter for Attracted and Repelled Particles where $\Phi_p = +100$ Volts and $\Phi_{particle} = \pm 100$ Volts. $\Phi_{particle}(\text{Gold.})$ refers to results obtained using eq.(2-35), and $\Phi_{particle}(\text{TPM})$ refers to results obtained using the TurningPoint program.	51
Figure 3.5. Radius from the Probe vs Impact Parameter for $\Phi_p = +100$ Volts and $\Phi_{particle} =$	

±10 Volts	52
Figure 3.6. Turning Angle vs Radius from the Probe and Impact Parameter	53
Figure 3.7. Turning Angle vs Impact Parameter for Attracted and Repelled Particles for the Case When $\phi(r) = \frac{\phi_p}{r}$, $\Phi_p = +100$ Volts	54
Table 3.1. Results from TurningPoint, $\phi_p = 20$	50
Table 3.2. Turning Moment, $\Phi_p = 100$ Volts	55

Nomenclature

A Area

a Particle acceleration

b Impact parameter

E Energy

E_0 Initial energy

e Electron charge

ε_0 Permittivity

F Force

g Turning point function

I Ion current

I_0 Constant ion current

i Dimensionless ion current, $i = \frac{I}{eN_\infty \sqrt{\frac{kT}{2\pi m}}}$

J Dimensionless angular momentum, $J = \frac{L}{\sqrt{2kTmR_p^2}}$

k Boltzmann constant

L Angular momentum

λ_D Debye length

λ_d Dimensionless Debye length, $\lambda_d = \frac{\lambda_D}{R}$

M_n Monoenergetic contribution to n

M_i	Monoenergetic contribution to i
m	Particle mass
N	Number density
N_∞	Ambient number density
n	Dimensionless number density, $n = \frac{N}{N_\infty}$
Φ	Electrical potential
Φ_0	Initial electrical potential
Φ_p	Probe electrical potential
$\Phi_{particle}$	Particle electrical potential
ϕ	Dimensionless electrical potential, $\phi = \frac{e\Phi}{kT}$
ϕ_∞	Dimensionless electrical potential at infinity (beyond the sheath)
ϕ_p	Dimensionless probe electrical potential
ϕ_{source}	Dimensionless electrical potential at the source
q	Partial particle charge
R	Radial position
R_{sheath}	Sheath radius
R_p	Probe radius
r	Dimensionless radial position, $r = \frac{R}{R_p}$
r_{sheath}	Dimensionless sheath radius
ρ	Net particle density

s	Sheath thickness
T	Particle temperature
t	Time
θ	Particle trajectory relative to the probe, or the turning angle
U	Effective potential
u	Average velocity
V	Particle velocity
V_r	Radial velocity
V_θ	Angular velocity
v	Dimensionless particle velocity, $v = \frac{V}{\sqrt{\frac{2kT}{m}}}$
x	Position

1. Introduction

1.1 Plasma Probe Theory Review

Modeling and prediction of current collection by a surface immersed in the space plasma finds important applications. A spacecraft immersed in a space plasma resembles a Langmuir probe – it collects charged particles from the plasma onto its surface, and that current collection depends on the spacecraft’s geometry and charge. Current collection onto a spacecraft surface can have negative consequences for the spacecraft, including surface charging, deep dielectric charging and material degradation [Hoyt, 2005]. Modeling and predicting the interaction between a plasma and a spacecraft is critical to ensuring the health of a spacecraft and the success of its mission.

Langmuir first proposed using a metal electrode (or probe) to measure the electron and ion currents in a plasma when various voltages are applied to the electrode as a way of analyzing the plasma’s basic characteristics – the current versus probe voltage curve that is produced is called the probe characteristic [Langmuir, 1926]. Langmuir probes of various shapes and sizes have been used for decades to analyze the characteristics of laboratory and space plasmas. [Hutchinson, 1987 and references therein]. The plasma characteristics of primary interest are the plasma charge and current density (or the collected probe current) and temperature. These parameters can be determined by analysis of the probe characteristics. A probe sheath is a charge boundary around the probe that separates the bulk of the plasma from the probe surface. The probe

sheath thickness and the sheath potential distribution are directly related to the plasma characteristics and can be used to determine properties of the plasma.

Understanding current collection by biased surfaces in space plasmas is also an important issue for successful operation of electrodynamic tethers. A space tether is one mass connected to another mass through a tether that serves to transfer either momentum or energy, or both, from one mass to the other in order to generate space propulsion without expending fuel, or to generate power from the radiated space environment [Tethers Unlimited, 2004]. An electrodynamic tether, or EDT, is a wire that extends from a spacecraft and collects and emits particles as it travels through the earth's magnetic field, from which the satellite can either generate thrust or power as necessary by exploiting the electro-dynamic interactions between the tether and the Earth's magnetic field. By understanding the probe sheath that forms around the EDT, one can determine how much current the tether is able to collect from the surrounding plasma and hence the efficiency of the tether.

Besides providing propulsion and power to a spacecraft, tethers also have the ability to deflect particles that enter the vicinity of the probe sheath. Charged particles from the sun or other radiation sources that enter the vicinity of the Earth will often drift and bounce between the poles along the Earth's magnetic field lines, effectively keeping the particles trapped between high boundary of low earth orbit (LEO) and geosynchronous earth orbit (GEO), a phenomenon known as the Van Allen radiation belts [Hoyt and Minor, 2005]. When a particle interacts with the sheath surrounding the tether, the particle is "turned" and the trajectory is altered. If the particle is deflected enough that its trajectory falls below a certain pitch angle (the angle between the velocity

vector and the geomagnetic field vector), known as the “loss cone”, it will follow the field lines down into the Earth’s upper atmosphere and scatter into the atmosphere. Knowing the turning angle of a particle in a sheath provides information about the efficiency of a tether’s particle deflection efforts and the strength of a tether needed to deflect particles of a certain energy into their loss cones.

Since Langmuir’s early work, other modern theories for predicting plasma/probe interactions have been proposed, including a widely used theory by Laframboise [Laframboise, 1966]. Laframboise’s theory states that, in a symmetrical central force, a particle’s initial energy and angular momentum are conserved along the particle’s orbit, enabling the two-body central-force equations to be used to determine the trajectory of a particle for different temperatures. This approach is used as the basis for the Effective Potential Method that Laframboise later developed, and the Turning Point Method developed by Parker [1976]. The two methods are physically identical and differ only in the order of the mathematical operations. The application of the Turning Point Method, or TPM, is the focus of this paper as a relatively simple and self-consistent method for analyzing plasma properties and particle trajectories.

1.1.1. Planar Langmuir Probes and the Planar Sheath

There are two well-known limits into which plasma probe theory falls. The first limit is when the sheath surrounding the probe is thin compared to the probe geometry and all, or nearly all, particles that enter the probe sheath hit the probe and contribute to the collected probe current. This limit is known as the planar limit. The second limit is when

the sheath is large, and only particles with an angular momentum below a certain threshold will intersect with the probe and contribute to the probe current. Both cases are illustrated in Figure 1.1.

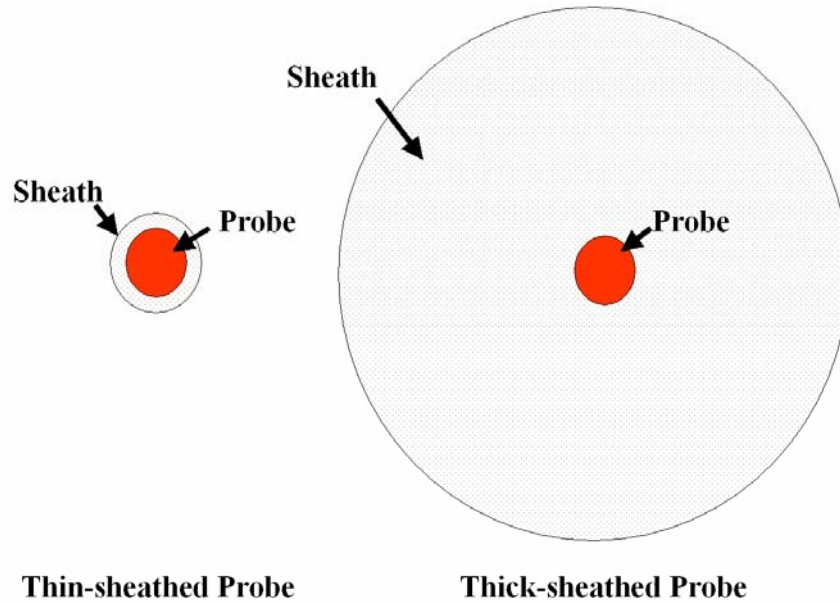


Figure 1.1. Thick- vs Thin-Sheathed Probes

To begin to understand probe theory and how the plasma potential, current density and sheath radius are related, it is first convenient to start with the simple case of a planar probe in a collisionless, isotropic and stationary plasma. A collisionless plasma refers to a plasma where the mean free path of the plasma particles is greater than the probe radius, r_p . A stationary and isotropic plasma refers to a plasma with an equal number of electrons and ions that are initially uniformly distributed, with no random thermal motion [Dendy, 1990]. Probe theory in a collisionless plasma is based on

combining two equations to produce one self-consistent solution. The first equation is Poisson's equation:

$$\nabla\Phi^2 = 4\pi e(N_e - N_i) = -\frac{\rho}{\epsilon_0} \quad (1-1)$$

where Φ is the electrical potential of the plasma, ρ is the net charge density, ϵ_0 is the permittivity of space, e is the electron charge, N_i is the ion density and N_e is the electron density. The second equation is Vlasov's equation (the collisionless Boltzmann equation) that describes the evolution of the distribution function $f(\vec{R}, \vec{V})$

$$\frac{\partial f}{\partial t} + \vec{V} \cdot \nabla_x f + \vec{a} \cdot \nabla_v f = 0 \quad (1-2)$$

where, ∇_x and ∇_v denote the gradient operator with respect to position and velocity space, and \vec{V} and \vec{a} are the velocity and acceleration of the particle, respectively. The zero-th moment of the Vlasov equation is defined as the density of a particle species (charged or otherwise) whose distribution of velocity is described by $f(\vec{R}, \vec{V})$, and is given by

$$N(\vec{R}) = \iiint f(\vec{R}, \vec{V}) d^p \vec{V} \quad (1-3)$$

where p is equal to 2 for a cylindrical probe, and 3 for a spherical probe [Parker, 1980]. The current density of a plasma, I , is defined as the first moment of the Vlasov equation and is given as eq. (1-4), using the same velocity distribution and terminology as eq.(1-3):

$$I = \iiint f(\vec{R}, \vec{V}) \vec{V} d^p \vec{V} \quad (1-4)$$

With the proper boundary conditions, it is possible to use Vlasov's equation to solve for the charge and current density given a known potential. Conversely, Poisson's equation can solve for the electric potential given a known charge density; hence, solving Poisson's and Vlasov's equations simultaneously will yield the current density and plasma potential.

When the sheath is very thin compared to the probe dimensions, a probe of cylindrical or spherical geometry can be modeled as a one-dimensional planar diode. In this case an analytical approximation of the plasma temperature and density can be made using what is called the Child-Langmuir Law [Leiberman and Lichtenburg, 1994]. Conservation of energy states that

$$E = e\Phi(R) + \frac{1}{2}mu^2(x) + E_0 . \quad (1-5)$$

m and $u(x)$ are the particle mass and the average velocity, and E_0 is the initial energy of the particle. Because the particle mass appears only once with the average velocity in eq. (1-5), both ions and electrons gain the same energy falling through the same potential field. Let's consider the case of a negatively charged probe, with ambient ions that have an initial energy that is negligible compared to the probe potential. The conservation of energy equation reduces to

$$-e\Phi(x) = \frac{1}{2}m_i u_i^2(x) . \quad (1-6)$$

Inside of the sheath the ion flux is constant, and is defined as

$$I_0 = eN_i(x)u(x) \quad (1-7)$$

where I_0 is the constant ion current. Solving for $N_i(x)$ and using Poisson's equation and the conservation of energy, we have

$$\frac{d^2\Phi}{dx^2} = -\frac{I_0}{\epsilon_0} \left(-\frac{2e\Phi}{m_i} \right)^{-1/2}. \quad (1-8)$$

At the sheath edge (where $x=0$), we can assume that the sheath potential is zero ($\Phi=0$) as well as the electric field ($\Phi'=0$). With these boundary conditions, integrating eq. (1-8) yields

$$\frac{1}{2} \left(\frac{d\Phi}{dx} \right)^2 = -\frac{I_0}{\epsilon_0} \left(\frac{-2e\Phi}{m_i} \right)^{1/2}.$$

If the equation is integrated again over x , the result is

$$\frac{4}{3} \Phi^{3/4} = 2^{3/4} x \left(\frac{I_0}{m_i \epsilon_0} \right)^{1/2}.$$

Letting $\Phi = -\Phi_p$ when $x = s$ results in a relationship between the sheath thickness, s , current density, I_0 , and probe potential, Φ_p , known as the Child-Langmuir Law, which states

$$I_0 = \frac{4}{9} \epsilon_0 \left(\frac{2e}{m_i} \right)^{1/2} \frac{\Phi_p^{3/2}}{s^2}. \quad (1-9)$$

Since the flux of ions is constant, the flux at the sheath edge is

$$eN_i u_i = eN_{i,sheath} u_{i,sheath}. \quad (1-10)$$

Equation (1-10) is known as the conservation of flux. When the ions are accelerating into the sheath, the ion density must decrease in order to maintain a constant flux. Since the sheath must maintain a positive charge in order to remain stable, the decrease of ion density must be slower than the decrease in electron density. Ion density is obtained by solving eq.(1-6) for $u_i^2(x)$ and substituting the result into eq.(1-10):

$$N_i = \frac{N_{i,sheath} u_{i,sheath}}{\sqrt{2e\Phi/m_i}}. \quad (1-11)$$

Since the electrons are repelled, they remain in equilibrium to the density everywhere, and the electron density at any point in the sheath is given by the Boltzmann relation:

$$N_e = N_{e,sheath} \exp\left(\frac{e\Phi}{kT_e}\right) \quad (1-12)$$

where k is the Boltzmann constant and T is the particle temperature; in this case T_e is the electron temperature. By imposing the condition that the ion density must fall off slower than the electron density, we can take the derivative of equations (1-11) and (1-12) (in relation to x) and set them equal when $\Phi = 0$ (at the sheath edge), and solve for the minimum ion velocity necessary for a positive sheath at the sheath edge [Leiberman and Lichtenburg, 1994]:

$$u_{sheath} \geq u_B = \sqrt{\frac{eT_e}{m_i}}. \quad (1-13)$$

Equation (1-13) is known as the Bohm sheath criterion. The continuity of ion flux (eq. 1-7) at the sheath edge can be rewritten using $u(x) = u_{sheath}$ as

$$I_0 = N_e \sqrt{\frac{kT_e}{2\pi m_i}}. \quad (1-14)$$

The Debye length is a characteristic length scale of a plasma over which a single charged particle has a significant influence on another charged particle. Beyond the Debye length, it is assumed that the cumulative effects of the surrounding plasma have a dominating influence over a charged particle located in that region. The Debye length is defined as

$$\lambda_D = \sqrt{\frac{\epsilon_0 k T_e}{N_\infty e^2}} \quad (1-15)$$

[Leiberman and Lichtenburg, 1994]. When the ion flux is given explicitly as eq.(1-14), the Child Law can be manipulated to give the sheath thickness in terms of the Debye length, λ_D , as

$$s = \frac{\sqrt{2}}{3} \lambda_D \left(\frac{\Phi_p e}{k T_e} \right)^{3/4}. \quad (1-16)$$

By determining the sheath thickness, it is possible to simultaneously solve for the plasma potential and collected probe current.

The Child Law is only valid when potentials inside the sheath are much larger than the surrounding ion and electron temperature, thereby contracting the sheath around the probe so that probes of varying geometries have sheaths thin enough that they can be modeled accurately as a planar diode. There are often situations where the Child law, which predicts $s \propto |\Phi_p - \Phi_{particle}|^{3/4}$, is not applicable; for instance, when $T_i \geq T_e$, or the probe voltage is low. In these cases, more general methods must be used to analyze the plasma that take into account different and more complex probe geometries.

1.1.2. Spherical and Cylindrical Langmuir Probes

Although the planar probe is a good starting point, all probes are finite and commonly have either spherical or cylindrical geometries because their symmetry allows for a mathematically tractable model. Specifically, a cylindrical Langmuir probe can be modeled as a wire of semi-infinite length (in the sense that edge effects can be ignored) to

ease analysis, and can accommodate sheath thicknesses that are much larger than the Debye length, in which the probe area, A , does not satisfy the condition $A \gg s^2$ [Leiberman and Lichtenburg, 1994].

The geometry of a spherical and cylindrical probe with respect to an incoming charged particle is shown in Figure 1.2, where R is the distance from the center of the probe to the particle, R_p is the probe radius and R_{sheath} is the sheath radius. V_θ is the angular velocity component, tangential to the radial velocity component V_R .

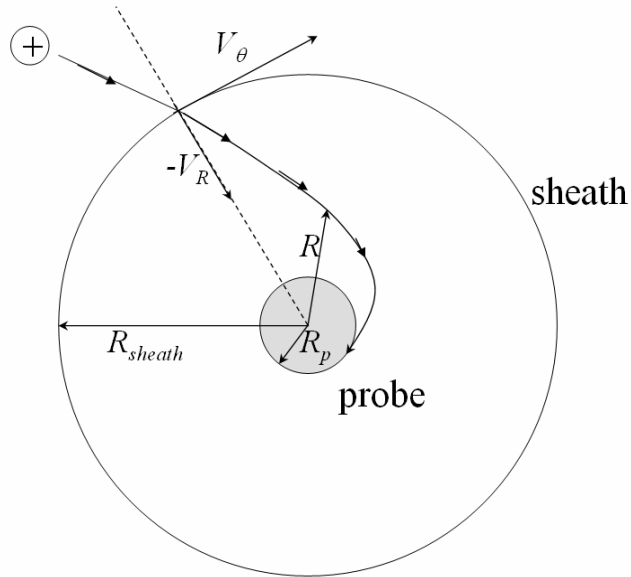


Figure 1.2. Trajectory of a Positively Charged Particle Around a Negatively Charged Probe

In each case the third dimension can be eliminated by symmetry – the z -direction along the cylinder and the azimuthal ρ -direction for the sphere. Thus we are left with the two-dimensional problem illustrated in Figure 1.2. By assuming that the plasma being

analyzed is isotropic and stationary, simplifications can be made that make evaluation of the plasma much simpler. With these assumptions all particle orbits, when traced back to infinity, have the same velocity distribution and retain their total energy throughout their entire orbit [Laframboise, 1966]. If the particle is also part of a two-body central-force system, the energy, E , and the angular momentum, L , remain constant throughout the entire trajectory of the particle, and are therefore considered constants of motion. L is defined as

$$L = mRV_{\theta} \quad (1-17)$$

and eq.(1-5) can be rewritten in terms of L as

$$E = e\Phi(R) + \frac{1}{2}mV_R^2 + \frac{L^2}{2mR^2}. \quad (1-18)$$

Not all of the orbital trajectories of each charged particle that enters the sheath will intersect with the probe surface if the sheath radius, R_{sheath} , is significantly larger than the probe radius, R_p , and V_{θ} is sufficiently large; therefore, a method must be developed that defines the boundaries of the constants of motion, E and L , that will result in a contribution to the charge density and therefore the collected probe current.

1.1.3. Plasma Analytical Methods

1.1.3.1. Orbit Motion Limited

When $R_p \gg \lambda_D$, the angular momentum of the particle (or its V_{θ} velocity component in Figure 1.2) is usually not important for all Φ because the sheath contracts closer to the

surface of the probe as the space charge increases – this is the condition where the Child Law is valid. When R_p is comparable to λ_D , the non-negligible space charge is dominated by ions that do not hit the probe. A probe theory must be used that can discriminate between the plasma charge density that contributes to the probe current and the charge density which does not.

One method for analyzing plasma characteristics is the Orbit Motion Limited theory, or OML. OML refers to the largest currents that can be collected by a perfectly absorbing spherical probe or an infinite-length cylindrical probe in a collisionless, stationary and isotropic plasma [Laframboise, 1973]. The total energy of a particle at infinity is $E = \frac{1}{2}mV^2$ if the potential energy at $\Phi(\infty) = 0$; therefore, particles coming in from infinity can only have energies of $E > 0$. At any position on the particle's orbit, its energy must be $E = \frac{1}{2}mV^2 + e\Phi(\bar{R}) > 0$, corresponding to a minimum speed component of $V > \left[\frac{-2e\Phi(\bar{R})}{m} \right]^{1/2}$. This criterion provides the boundary conditions needed to derive expressions for the charge and current density and the plasma potential.

A spherical probe can be modeled as a three-dimensional steady-state potential well, where a particle with a charge e has the potential $e\Phi(x, y, z) \leq 0$, with $\Phi \rightarrow 0$ as $x^2 + y^2 + z^2 \rightarrow \infty$. The number density of the plasma at any point on the particle's orbit was defined in eq.(1-3) and can be found analytically by integrating the Maxwellian distribution function, f , over velocity space and using the previous criteria as boundary conditions. Doing this, we obtain:

$$N(\bar{R}) = \int f(\bar{R}, \bar{V}) d^3\bar{V} \quad ; \quad f(\bar{R}, \bar{V}) = \left(\frac{m}{2\pi kT} \right)^{3/2} \exp\left(\frac{-mV^2}{2kT} \right) \quad (1-19)$$

$$N = N_\infty \left(\frac{m}{2\pi kT} \right)^{3/2} \exp\left(\frac{e\Phi}{kT} \right) \times \int_{(-2e\Phi/m)^{1/2}}^{\infty} \exp\left(\frac{-mV^2}{2kT} \right) 4\pi V^2 dV. \quad (1-20)$$

Integrating the above equation, we get the dimensionless number density, n :

$$n = \frac{N}{N_\infty} = \frac{2}{\sqrt{\pi}} \left[\phi^{1/2} + h(\phi^{1/2}) \right] \geq 1 \quad (1-21)$$

where

$$\phi = \frac{-e\Phi}{kT} \quad \text{and} \quad h(\phi) = \frac{1}{2} \pi^{1/2} \exp(\phi^2) \operatorname{erfc}(\phi) = \exp(\phi^2) \int_{\phi}^{\infty} \exp(-t^2) dt.$$

For a cylindrical probe, or a two-dimensional steady-state potential well, the minimum

speed component is $V = (V_x^2 + V_y^2)^{1/2} > \left[\frac{-2e\Phi(\bar{R})}{m} \right]^{1/2}$, in which case $\Phi \rightarrow 0$ as

$x^2 + y^2 \rightarrow \infty$. The resulting number density is

$$\begin{aligned} n &= \frac{N}{N_\infty} = \left(\frac{m}{2\pi kT} \right)^{3/2} \exp\left(\frac{-e\Phi}{kT} \right) \int_{-\infty}^{\infty} \exp\left(\frac{-mV_x^2}{2kT} \right) dV_x \times \int_{(-2e\Phi/m)^{1/2}}^{\infty} \exp\left(\frac{-mV^2}{2kT} \right) 2\pi V dV \\ &= 1. \end{aligned} \quad (1-22)$$

The result of $n = 1$ for a cylindrical probe is due to the fact that the density increase due to the concentrating effect of the probe geometry is exactly compensated for by the density decrease due to particle acceleration across the sheath [Laframboise, 1973].

Figure 1.3 below shows the dimensionless number density, n , plotted against the dimensionless potential, ϕ .

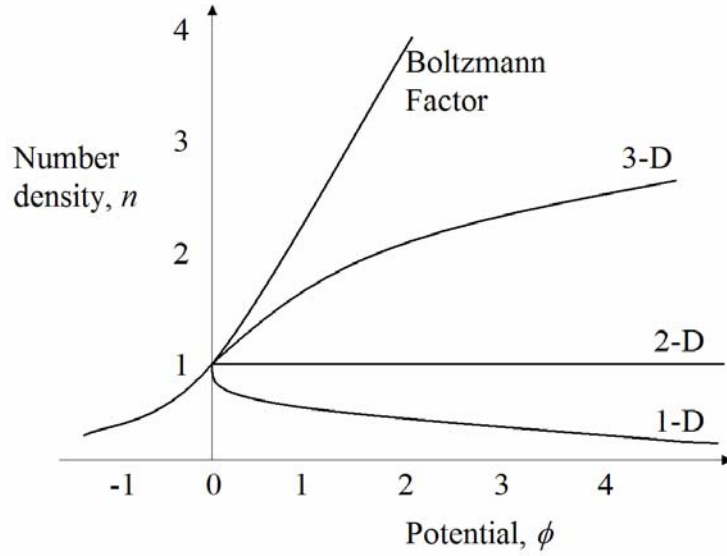


Figure 1.3: Number Density n vs Potential ϕ

The current density of a plasma, I , was defined as eq.(1-4). For the three-dimensional case of a spherical probe, the current is given by

$$\begin{aligned}
 I &= \iiint f(\vec{R}, \vec{V}) \vec{V} d^3V \\
 &= \left(\frac{m}{2\pi kT} \right)^{3/2} \exp\left(\frac{-e\Phi}{kT} \right) \times \int_{\psi=0}^{\psi=2\pi} d\psi \int_{\theta=0}^{\theta=\pi/2} \sin\theta \cos\theta d\theta \int_{V=(-2e\Phi/m)^{1/2}}^{V=\infty} \exp\left(\frac{-mV^2}{2kT} \right) V^3 dV \\
 &= I_0(1 + \phi) \tag{1-23}
 \end{aligned}$$

where I_0 is defined as eq.(1-14). For the two-dimensional case of a cylindrical probe, the current is

$$\begin{aligned}
 I &= N_\infty \left(\frac{m}{2\pi kT} \right) \exp\left(\frac{-e\Phi}{kT} \right) \times \int_{V=(-2e\Phi/m)^{1/2}}^{V=\infty} \exp\left(\frac{-mV^2}{2kT} \right) V^2 dV \int_{\theta=0}^{\theta=\pi/2} \cos\theta d\theta \int_{-\infty}^{\infty} \exp\left(\frac{-mV_x^2}{2kT} \right) dV_x \\
 &= I_0(2/\pi^{1/2}) \left[\phi^{1/2} + h(\phi^{1/2}) \right]. \tag{1-24}
 \end{aligned}$$

For different values of current and potential, the cylindrical and the spherical probes exhibit the behavior shown in Figure 1.4:

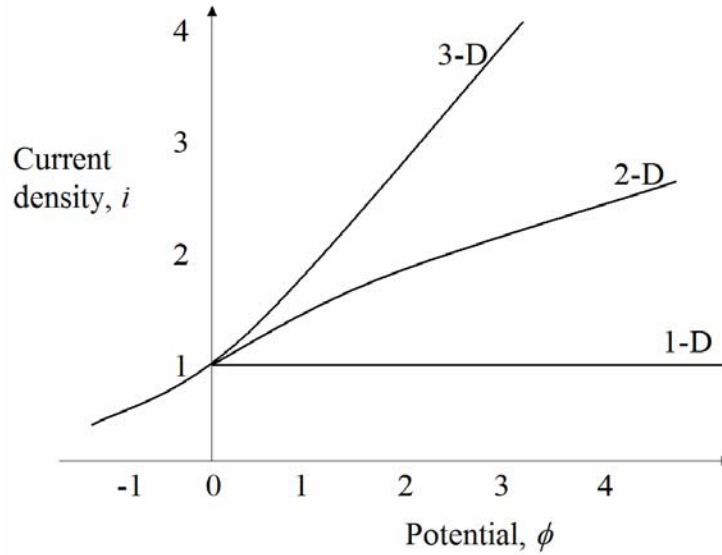


Figure 1.4: Current Density i vs Potential ϕ

The OML theory is useful for predicting plasma current and potential because numerical results are easy to obtain given the simple equations derived from the OML criteria. However, as we will discover in the following chapters, the OML theory has a significant limitation such that the method is only accurate for a probe radius either equivalent to or smaller than the Debye length of the plasma; for a spherical probe, the

probe only becomes orbit-limited as $\frac{R_p}{\lambda_D} \rightarrow 0$, while for a cylindrical probe the orbit-

limited case holds until $\frac{R_p}{\lambda_D} \approx 1$ [Laframboise, 1973]. Consequently, a more robust

method must be used for analyzing probes in plasmas where $\frac{R_p}{\lambda_D} > 1$.

1.1.3.2. Effective-Potential Formulation

It would be to our advantage to express the Poisson and Vlasov equations in terms of the constants of motion, since they completely characterize a particle's orbit. Attracted particles in the plasma surrounding the probe will either penetrate the sheath (charge boundary) and be absorbed by the probe or pass by the probe; repelled particles will either penetrate the sheath and either hit or pass by the probe or not be able to penetrate the sheath at all. A method must be developed that defines the boundaries of the constants of motion, E and L , that will result in a contribution to the charge density and therefore the collected probe current. One way to define the proper boundaries for E and L is to use what is called the Effective-Potential Formulation developed by Laframboise [Laframboise, 1973]. The Effective-Potential Formulation classifies the particle orbits and their contributions to the charge density by defining an effective potential,

$$U = -e\Phi + \frac{L^2}{2mR^2},$$
 for which particles must have a certain energy E greater than U in

order to represent a particle which can strike or pass by the probe. If E is less than U , then the particle will not penetrate the sheath. The relation $E = U$ is a straight line in the (E, L^2) plane that defines which particles will strike the probe, pass by the probe, or cannot penetrate the sheath. When considering a sheath around the probe, the effective potential U varies as a function of L^2 with changing R . The Effective-Potential Formulation finds the first two derivatives of U (with respect to R) and, plotted in the (E, L^2) plane, classifies unpopulated orbits above the curve and populated orbits below the curve.

1.1.3.3. Turning Point Method

Another way to determine the boundaries of E and L is to use the Turning Point Method, or TPM, which was developed by Parker as an alternative to Laframboise's earlier Effective-Potential Formulation [Parker, 1980]. The conservation of energy equation can be rewritten in dimensionless terms as

$$E = \phi + v_r^2 + \frac{J^2}{r^2} \quad (1-25)$$

where $\phi = \frac{e\Phi}{kT}$, $v = \frac{V}{\sqrt{\frac{2kT}{m}}}$, $J = \frac{L}{\sqrt{2kTmR_p}}$, and $r = \frac{R}{R_p}$; in this case, $v_r = \frac{V_R}{\sqrt{\frac{2kT}{m}}}$. The

TPM defines a turning point as the point where the radial velocity component $v_r = 0$. Consequently, a particle will not vanish or change sign (i.e. a particle will exist) as long as

$$E > \phi + \frac{J^2}{r^2} \quad (1-26)$$

or

$$J^2 < g \equiv r^2(E - \phi) \quad (1-27)$$

In the above equation, g is defined as the turning point function. When g is plotted in the (J^2, r) plane, all physically possible orbits exist below the turning point function curve. The TPM has an advantage over the Effective Potential Formulation in that the turning point function g can have any number of inflections (or charge boundaries) while the effective potential function U contains no more than two maxima. Also, the Effective

Potential Formulation assumes that the potential function is monotonic, while the turning point function can be monotonic or nonmonotonic [Parker, 1980].

1.2. Review of Particle-In-Cell Computational Model

Various forms of particle-in-cell (PIC) computation have been used to perform the detailed numerical calculations necessary for modeling plasma physics related to current collection by probes. The general computational cycle of PIC is outlined below. In PIC, a spatial grid is used with cells on the order of the Debye length of the plasma. The charge density, electric field and electric potential at each point on the grid are evaluated. The grid also provides a smoothing effect by not including spatial fluctuations smaller than the Debye length of the plasma.

The general computational cycle flows in the following order: 1) Integrate the equations of motion to find the particle's position; 2) Use a system based on the particle position to calculate the charge density and current using the values from the equations of motion (called "weighting"); 3) Use the calculated charge current and density to integrate and solve the field equations and find the electric and magnetic fields; 4) Perform an inverse weighting to apply the field values on the grid to the next particle on the spatial grid; 5) Repeat steps 1) through 4) for every grid point [Birdsall and Langdon, 1985].

The "leap-frog method" for calculating F , V and x is a commonly used method for integration of the equations of motion because it allows for the two first-order differential equations of motion to be integrated separately. This method is the most efficient way to "time center" the steps and minimize the error. The velocity and position of the particle

aren't known at the same time and are calculated at different time intervals (hence the leap-frog name), as is illustrated in Figure 1.5.

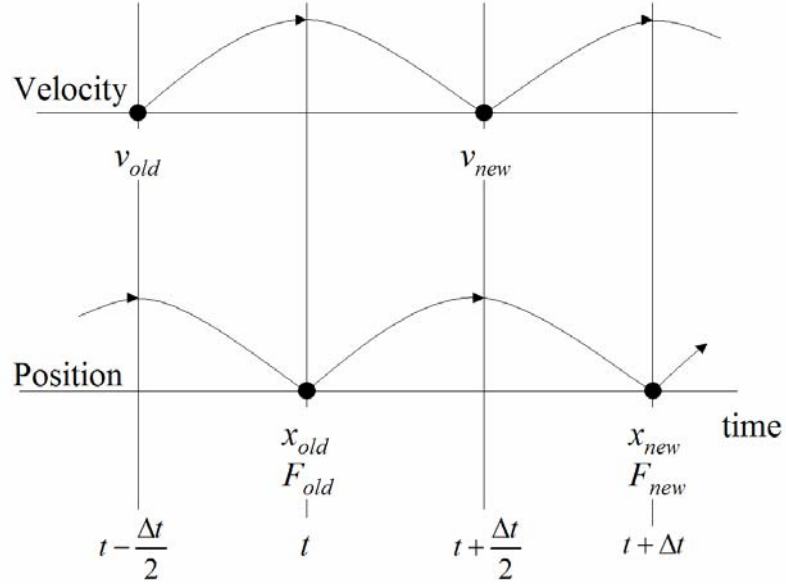


Figure 1.5: The leap-frog method for calculating the force F while advancing V , and V while advancing x

From the equations of motion $\vec{F} = m \frac{d\vec{V}}{dt}$ and $\vec{V} = \frac{d\vec{x}}{dt}$, the finite-difference equations are

$$\frac{x_{new} - x_{old}}{\Delta t} = V_{new} \rightarrow m \frac{V_{new} - V_{old}}{\Delta t} = F_{old},$$

constituting the leap-frog integration method of time-centering the force F while advancing V , and of V while advancing x , resulting in the positions and fields being calculated at integer time-steps while the velocity calculations are offset from the position calculations by half time-steps.

When integrating the field equations, charges and current densities are calculated at the grid points using a weighting system specified by the user. The electric field, E , is

calculated again at each point with Poisson's equation, eq.(1-1), using the charges and densities calculated in the second step. The finite-difference equations for the field equations are

$$E_j = \frac{\phi_j - \phi_{j-1}}{\Delta x} \quad \text{and} \quad \nabla \cdot E_j = \frac{\phi_{j-1} - 2\phi_j + \phi_{j+1}}{(\Delta x)^2} = -\frac{\rho}{\epsilon_0}.$$

If the boundary conditions are known, there will be the same number of equations as unknowns, and the ϕ 's are therefore solvable.

Weighting is used to calculate the charge density on the discrete grid points from the particle positions and, after the fields are obtained, to calculate the force at the particles from the fields at the grid points by interpolating between the grid points nearest the particle. The charge density is typically calculated inside of the cell (between grid points), while the force, E , is calculated at the grid points. PIC is often used to model charged particles subjected to electric fields and inter-particle forces, either with collisions (using a Monte-Carlo simulation) or without collisions, and is particularly applicable to modeling non-equilibrium plasmas, where the particles do not follow a distribution that is a constant function of the local fields. However, the drawback of using PIC is that it is computationally intensive, as well as being sensitive to random density and field variations (noise).

1.3. Objectives and Methodology

Current plasma models employ complicated algorithms for analyzing plasma characteristics as realistically as possible, taking into account many factors such as

particle collisions, multiple charge boundaries (multiple sheaths), trapped particles, interacting magnetic fields, etc., while maintaining efficiency. As a result of so many variables, it's difficult to determine if a specific plasma theory or code is producing the "right" answer, or an answer that accurately predicts the behavior of a real-life plasma. A classical solution that provides a straightforward analysis of a problem is desirable to compare with more complicated analytical techniques. For plasma analysis, a "classical" model that uses a minimum of well-constrained variables for an easily reproducible numerical result is needed that provides standards for validation of the more complex models that includes space charge. This thesis seeks to provide that "classical" plasma model for validation of other models by creating a computer program that solves the Poisson and Vlasov problems with a TPM Vlasov solution.

The TPM provides an ability to identify the point where a particle turns in its orbit. By knowing where a particle turns in its orbit, the entire trajectory of the particle can be traced to and from infinity without having to know any other information about the particle's orbit. This provides a much simpler alternative to the computationally intensive PIC weighting method, which must calculate the entire trajectory of the particle. The TPM also provides a straightforward method for determining the turning angle of a particle along its orbit. By definition, the TPM identifies the position at which a particle of a certain energy will achieve a maximum trajectory deflection angle in a potential field, relative to its initial trajectory, which we will refer to as the turning angle, θ . A particle with an angular momentum of J will make its closest approach to the probe at a radius r where it intersects with the turning function (below the curve), g , and continues out to infinity along a trajectory symmetrical to its incoming path.

This thesis will specifically look at the case of a charged particle either attracted or repelled to a charged cylindrical probe by using a computer code originally developed by Cooke [Cooke, 1981], following the method outlined by Parker [Parker, 1980]. The original program used Fortran code to model the characteristics of particles that are either attracted to or repelled by a spherical probe using the TPM. In this effort, the code was expanded to include the analysis of cylindrical probe geometry, as well as an added subroutine that finds the turning angle of the charged particle (repelled or attracted) around the probe.

2. Turning Point Method and Computer Program Structure

2.1. The Turning Point Method

The Turning Point Method was developed by Parker [1980] to determine the characteristics of current collection by a probe in a collisionless, isotropic and stationary plasma with an arbitrary radius compared to the plasma Debye length, although it is most useful for probe radii that are 1 to 100 times the Debye length. To find the current density and potential, two governing equations are used – Poisson’s equation, eq.(1-1), and Vlasov’s equation, eq.(1-2). The time-independent form of Vlasov’s equation is given as

$$\vec{V} \cdot \nabla_R f + \frac{q}{m} \nabla_R \Phi \cdot \nabla_V f = 0 \quad (2-1)$$

In eq.(2-1), q is the charge of the particle. In this analysis we assume the velocity distribution, f , to be Maxwellian for both electrons and ions. With the proper boundary conditions, it is possible to manipulate Vlasov’s equation in order to solve for the particle density, known as the “Vlasov Problem”; conversely, Poisson’s equation can be solved to yield the electrical potential given a constant particle density, known as the “Poisson Problem”. By solving the Vlasov Problem and the Poisson Problem iteratively on a set of grid points, the particle (and therefore current) density and the plasma potential can be determined. Once the plasma’s potential distribution is determined, the turning angle of any particular particle with a given energy and impact parameter can also be calculated.

2.1.1. The Vlasov Problem

We do not solve the Vlasov equation directly; rather, we use the result which is that the distribution function is constant along the particle trajectory. It is important to note that this is true for some small interval in velocity space about the trajectory. This allows us to build the total distribution function at a point from a collection of distinct contributing functions and velocity space boundaries that classifies the particle orbits into whether or not they contribute to the current density measured by the probe.

In terms of v and θ , the particle density, N , as defined in eq.(1-20) can be written in dimensionless form:

$$n = \frac{2}{\sqrt{\pi}} \int_{v_{\min}}^{\infty} \exp(-v^2 - \phi) v^2 dv \int d(\cos \theta) \quad (2-2)$$

for spherical coordinates, and

$$n = \frac{2}{\sqrt{\pi}} \int_{v_{\min}}^{\infty} \exp(-v^2 - \phi) v dv \int d\theta \quad (2-3)$$

for cylindrical coordinates, assuming a Maxwellian velocity distribution.

In this form, the limits of integration over θ are unknown. The goal of the following analysis is to define these limits and thereby derive expressions for the charge and current density.

The evaluation of the particle density can be simplified by transforming the integration of n over v and θ into integration over the constants of the motion, E and J , so called because E is conserved in steady state motion and J is conserved in a central force problem. The constants of motion in dimensionless form are

$$E = v^2 + \phi \quad \text{and} \quad J = rv \sin \theta. \quad (2-4)$$

When the dimensionless energy and angular momentum defined in eq.(2-4) are substituted into eq.(2-2) and (2-3), the charge density n can be transformed into

$$n = \frac{2}{\pi} \exp(\phi_{source}) \int_{E_{min}}^{\infty} \exp(-E) dEM_{ns}(E) \quad (2-5)$$

for spherical probes and

$$n = \exp(\phi_{source}) \int_{E_{min}}^{\infty} \exp(-E) dEM_{nc}(E) \quad (2-6)$$

for cylindrical probes.

ϕ_{source} is the potential at the source, which is ϕ_{∞} for ambient particles and zero otherwise [Parker, 1980]. M_n is the “monoenergetic” contribution (contributions to the density or flux for a given energy) to n , defined as

$$\begin{aligned} M_{ns}(E) &= \frac{C}{2} \sqrt{E - \phi} \int_{-1}^1 \delta(\cos \theta) \\ &= \frac{C}{2} \int_0^{\sqrt{E - \phi}} \delta d \left(E - \phi - \frac{J^2}{r^2} \right)^{\frac{1}{2}} \end{aligned} \quad (2-7)$$

for spherical probes and

$$\begin{aligned} M_{nc}(E) &= \frac{C}{\pi} \int_0^{\pi} \delta d \theta \\ &= \frac{C}{\pi} \int_0^{\pi} \delta d \left\{ \sin^{-1} \left[\frac{J^2}{r^2} (E - \phi) \right] \right\}^{\frac{1}{2}} \end{aligned} \quad (2-8)$$

for cylindrical probes, where E is held constant and the integrals are evaluated over J^2 . The factor C is unity for ambient particles and 2 for emitted particles (the factor 2 is associated with a half-Maxwellian of emitted particles at the surface, there being only outgoing trajectories when there is no electric field). The factor δ gives orbit information defining what source a particle in a certain orbit will connect with. For ambient particles, $\delta = 1$ if the particle comes from infinity and $\delta = 0$ if it comes from the probe surface. Similarly, for emitted particles, $\delta = 0$ if the particle comes from infinity and $\delta = 1$ if it comes from the surface. Simply put, a nonzero value for δ means that an orbit is “occupied”. Defining which particles have an angular momentum that contribute to the collected probe current and which do not makes it possible to define M_n . This is where the TPM comes in.

In a symmetric, central-force potential, four types of orbits can exist as illustrated in Figure 2.1:

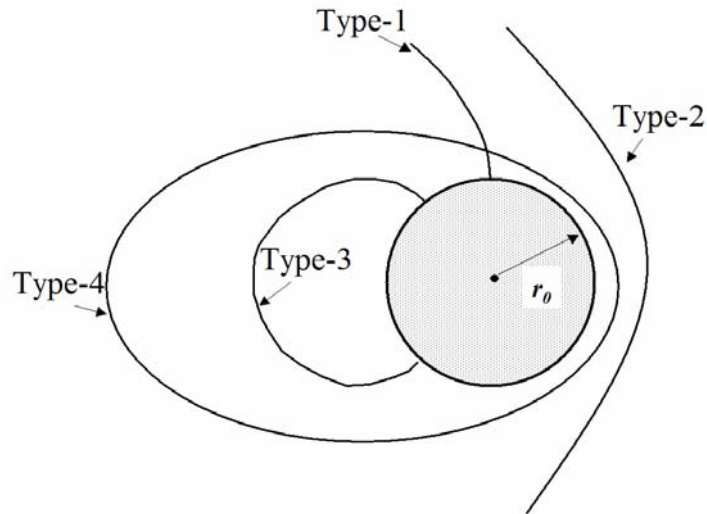


Figure 2.1: The 4 Types of Orbits

Type 1: Orbits that include ambient particles that pass from infinity to the probe, or emitted particles that pass from the probe to infinity. These orbits have no turning point and $\delta = 1$.

Type 2: Orbits that include ambient particles that pass from infinity by the probe at a minimum radius without intersecting the probe surface, and back out to infinity again. These particles have one turning point and a delta factor of $\delta = 2$ to account for the ingoing and outgoing trajectory contributions of the particle.

Type 3: Orbits that comprise of particles emitted from the surface of the probe that travel out to a maximum radius and then return back to the probe surface. Particles in type 3 orbits have one turning point and a delta factor of $\delta = 2$ to account for the ingoing and outgoing trajectory of the particle.

Type 4: Closed or “trapped” orbits where particles circle the probe indefinitely without making contact with the surface. These orbits are assumed to be unpopulated in collisionless plasmas and therefore $\delta = 0$ for them.

From analysis of the orbit types, it is evident that type-1 and type-2 orbits can contribute to the plasma density simultaneously, and type-1 and type-3 orbits can contribute simultaneously, but type-2 and type-3 orbits cannot contribute simultaneously (as defined by its δ value – orbits with the same δ value cannot contribute simultaneously). Also, there will always be contributions by type-1 orbits between the

lowest value of J^2 and $J^2 = 0$. Hence, there can be orbits populated by either type-2 or type-3 orbits above the minimum J^2 .

From this analysis, equations (2-7) and (2-8) can be solved to define M_n for ambient or surface-emitted particles for either a spherical or cylindrical probe.

Spherical Probe

Ambient M_{na} is

$$M_{na}(E) = \left[-M_{gs}(J_{B1}^2) + M_{gs}(J_{A1}^2) \right] + 2 \left[-M_{gs}(J_{B2}^2) + M_{gs}(J_{A2}^2) \right]. \quad (2-9)$$

Type-1 orbits

Type-2 Orbits

Surface-emitted M_{ne} is

$$M_{ne}(E) = 2 \left[-M_{gs}(J_{B1}^2) + M_{gs}(J_{A1}^2) \right] + 4 \left[-M_{gs}(J_{B3}^2) + M_{gs}(J_{A3}^2) \right] \quad (2-10)$$

Type-1 Orbits

Type-3 Orbits

$$\text{where } M_{gs}(J^2) = \frac{1}{2r} \left[r^2(E - \phi) - J^2 \right]^{1/2} = \frac{(g - J^2)^{1/2}}{2r}. \quad (2-11)$$

Cylindrical Probe

Ambient M_{na} is

$$M_{na}(E) = \left[M_{gc}(J_{B1}^2) - M_{gc}(J_{A1}^2) \right] + 2 \left[M_{gc}(J_{B2}^2) - M_{gc}(J_{A2}^2) \right]. \quad (2-12)$$

Type-1 Orbits

Type-2 Orbits

Surface-emitted M_{ne} is

$$M_{ne}(E) = 2 \left[M_{gc}(J_{B1}^2) - M_{gc}(J_{A1}^2) \right] + 4 \left[M_{gc}(J_{B3}^2) - M_{gc}(J_{A3}^2) \right] \quad (2-13)$$

Type-1 Orbits

Type-3 Orbits

$$\text{where } M_{gc}(J^2) = \frac{1}{\pi} \sin^{-1} \left[\frac{J^2}{r^2(E-\phi)} \right]^{1/2} = \frac{1}{\pi} \sin^{-1} \left(\frac{J^2}{g} \right)^{1/2}. \quad (2-14)$$

In these equations, J_{A1}^2 , J_{A2}^2 and J_{A3}^2 denote, respectively, the lower limit (A) of type-1, type-2 and type-3 orbits, and J_{B1}^2 , J_{B2}^2 and J_{B3}^2 denote the upper limit (B) of type-1, type-2 and type-3 orbits.

To determine the values of J_{A1}^2 , J_{A2}^2 , J_{A3}^2 , J_{B1}^2 , J_{B2}^2 and J_{B3}^2 , the turning point function, g (eq.1-26), is plotted in the (J^2, r) plane and the minimum values of g are analyzed in relation to the radial position, r , at which they occur. Three cases are considered: case A – there is only one minimum value of $g(r)$ (known as the “absorption radius”, in this case at point a), case B – there is one secondary minima value of $g(r)$ before the absorption radius (point b is the absorption radius in this case), and case C – there is one secondary minima value of $g(r)$ after the absorption radius (point a is the absorption radius in this case). The three cases are illustrated in Figure 2.2.

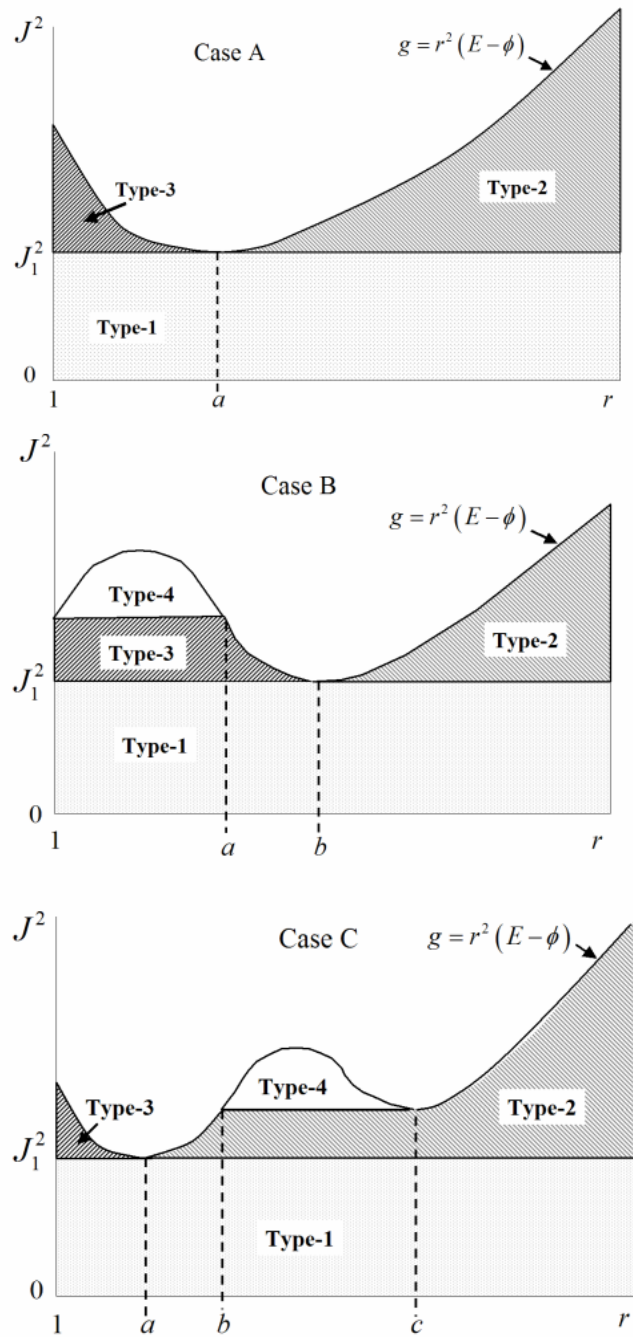


Figure 2.2: Case A, B, and C in r, J^2 space

In case A, the minimum of g occurs at point a , and corresponds to the minimum value of $J^2 = J_1^2$. Only type-1 orbits exist between $J^2 = 0$ and $J^2 = J_1^2$ and, since type-2

orbits are outside of the absorption radius, and type-3 orbits are inside the absorption radius, we have

Case A: For $r(1,a)$, $J_{A1}^2 = 0$, $J_{B1}^2 = J_{A3}^2 = J_1^2$, $J_{B3}^2 = g(r) \rightarrow$ no type-2 orbits

For $r(a,\infty)$, $J_{A1}^2 = 0$, $J_{A2}^2 = J_1^2$, $J_{B2}^2 = g(r) \rightarrow$ no type-3 orbits

In case B, the minimum of g occurs at point b with a secondary minima at $r = 1$, before point b . Therefore,

Case B: For $r(1,a)$, $J_{A1}^2 = 0$, $J_{B1}^2 = J_{A3}^2 = J_1^2$, $J_{B3}^2 = g(a) \rightarrow$ no type-2 orbits

For $r(a,b)$, $J_{A1}^2 = 0$, $J_{B1}^2 = J_{A3}^2 = J_1^2$, $J_{B3}^2 = g(r) \rightarrow$ no type-2 orbits

For $r(b,\infty)$, $J_{A1}^2 = 0$, $J_{B1}^2 = J_{A2}^2 = J_1^2$, $J_{B2}^2 = g(r) \rightarrow$ no type-3 orbits

In case C, the minimum value of g occurs at point a , while a secondary minima occurs after point a at point c :

Case C: For $r(1,a)$, $J_{A1}^2 = 0$, $J_{B1}^2 = J_{A3}^2 = J_1^2$, $J_{B3}^2 = g(r) \rightarrow$ no type-2 orbits

For $r(a,b)$, $J_{A1}^2 = 0$, $J_{B1}^2 = J_{A2}^2 = J_1^2$, $J_{B2}^2 = g(r) \rightarrow$ no type-3 orbits

For $r(b,c)$, $J_{A1}^2 = 0$, $J_{B1}^2 = J_{A2}^2 = J_1^2$, $J_{B2}^2 = g(c) \rightarrow$ no type-3 orbits

For $r(c,\infty)$, $J_{A1}^2 = 0$, $J_{B1}^2 = J_{A2}^2 = J_1^2$, $J_{B2}^2 = g(r) \rightarrow$ no type-3 orbits

Now that the limits of J^2 are defined, equations (2-9), (2-10), (2-12) and (2-13) can be solved.

For a spherical probe, M_{ns} is

$$M_{ns}(E) = \frac{C}{2} \left[(E - \phi)^{1/2} - 2 \left(E - \phi - \frac{J_m^2}{r^2} \right)^{1/2} + \left(E - \phi - \frac{J_m^2}{r^2} \right)^{1/2} \right]. \quad (2-15)$$

For a cylindrical probe, M_{nc} is:

$$M_{nc}(E) = \frac{C}{\pi} \left[2 \sin^{-1} \left(\frac{J_m^2}{r^2(E - \phi)} \right)^{1/2} - \sin^{-1} \left(\frac{J_1^2}{r^2(E - \phi)} \right)^{1/2} \right]. \quad (2-16)$$

As described earlier, C is unity for ambient particles and 2 for surface-emitted particles. The subscript m in the variable J_m represents the upper boundary for the orbit type; for instance, $m = 1$ if there are only type-1 orbits, $m = 2$ if there are type-2 orbits (corresponding to ambient particles), and $m = 3$ if there are type-3 orbits (corresponding to emitted particles). For example, in the case of a probe in a plasma with monoenergetic ambient attracted particles similar to case A, the monoenergetic contribution to the particle density is as follows:

For a spherical probe

$$M_{ns}(E) = \frac{1}{2} \left[(E - \phi)^{1/2} - \left(E - \phi - \frac{J_1^2}{r^2} \right)^{1/2} \right] \quad \text{for } r \text{ in (1,a)}$$

$$M_{ns}(E) = \frac{1}{2} \left[(E - \phi)^{1/2} + \left(E - \phi - \frac{J_1^2}{r^2} \right)^{1/2} \right] \text{ for } r \text{ in } (a, \infty).$$

For a cylindrical probe

$$M_{nc}(E) = \frac{1}{\pi} \sin^{-1} \left[\frac{J_1^2}{r^2} (E - \phi) \right]^{1/2} \text{ for } r \text{ in } (1, a)$$

$$M_{nc}(E) = 1 - \frac{1}{\pi} \sin^{-1} \left[\frac{J_1^2}{r^2} (E - \phi) \right]^{1/2} \text{ for } r \text{ in } (a, \infty).$$

Now that the monoenergetic contribution to the particle density can be determined, it can be used to solve for the current density, I , the first moment of the Vlasov equation for a particle species with a velocity distribution function of $f(\vec{R})$ is defined as eq.(1-4).

Expressing the current density in a dimensionless form, where $i = \frac{I}{eN_\infty \sqrt{\frac{kT}{2\pi m}}}$, yields

$$i = 2 \int_{v_{\min}}^{\infty} \exp(-v^2 - \phi) v^3 dv \int d(\sin^2 \theta) \quad (2-17)$$

for a spherical probe, and

$$i = \frac{4}{\sqrt{\pi}} \int_{v_{\min}}^{\infty} \exp(-v^2 - \phi) v^2 dv \int d(\sin \theta) \quad (2-18)$$

for a cylindrical probe.

Applying the same technique used to transform the particle density, the current density is expressed in terms of the constants of motion, E and J^2 , as

$$i = \exp(\phi_{source}) \int_{E_{min}}^{\infty} \exp(-E) dEM_{is}(E) \quad (2-19)$$

for a spherical probe, and

$$i = \frac{2}{\sqrt{\pi}} \exp(\phi_{source}) \int_{E_{min}}^{\infty} \exp(-E) dEM_{ic}(E) \quad (2-20)$$

for a cylindrical probe.

Using the same methods to evaluate the monoenergetic contributions to current density as were used for evaluation of the monoenergetic contribution to particle density, M_{is} and M_{ic} are defined as

$$M_{is}(E) = \int_0^{E-\phi} \delta d \left(\frac{J^2}{r^2} \right) = \frac{J_1^2}{r^2} = J_1^2 \quad (2-21)$$

and

$$M_{ic}(E) = \int_0^{\sqrt{E-\phi}} \delta d \left(\frac{J^2}{r^2} \right)^{1/2} = \left(\frac{J_1^2}{r^2} \right)^{1/2} = J_1 . \quad (2-22)$$

In both cases, $r = 1$ since the current density of interest is that collected at the probe surface.

To finish solving the Vlasov Problem, the integrals over energy in equations (2-5), (2-6), (2-19) and (2-20) must be numerically evaluated. One approach for doing this is to use a quadrature formula in the form

$$\int_{E_{\min}}^{\infty} \exp(-E) dEM(E) = \sum_{z=1}^Z C_z M(E_z) \quad (2-23)$$

where C_z is a constant that varies with the energy E_z from $z = 1, 2, \dots, Z$. C_z and E_z are evaluated by establishing a minimum and maximum of the potential distribution, E_{\min} and E_{\max} . The integral can now be split up into two parts, one in the finite range of (E_{\min}, E_{\max}) and one in the semi-infinite range of (E_{\max}, ∞) :

$$\int_{E_{\min}}^{\infty} \exp(-E) dEM(E) = \int_{E_{\min}}^{E_{\max}} \exp(-E) dEM(E) + \int_{E_{\max}}^{\infty} \exp(-E) dEM(E). \quad (2-24)$$

The finite range consists of type-3 and type-4 orbits. When only considering type-1 and type-2 orbits (or only case A scenarios), $E_{\min} = E_{\max}$ and only the semi-infinite range applies. For the purpose of this paper, only a numerical solution of case A will be discussed here.

For the Maxwellian case where the integrand contains a Gaussian function as a weighted function, the coefficients C_z and E_z can be transformed into an abscissa-coefficient pair defined from the data of Steen et al. [Steen, 1969], and the semi-infinite range integral becomes

$$\begin{aligned} \int_{E_{\max}}^{\infty} \exp(-E) dEM(E) &= \exp(-E_{\max}) \int_0^{\infty} \exp(-U) dUM(U + E_{\max}) \\ &= \sum_{z=1}^Z 2H_z a_z \times M(a_z^2 + E_{\max}). \end{aligned} \quad (2-25)$$

Here, $C_z = 2H_z a_z$ and $E_z = a_z^2 + E_{\max}$, where H_z and a_z are the abscissa-coefficient pair defined in Steen et al. [1969].

This completes the procedure for solving the Vlasov Problem, which is the calculation of the densities and currents when the potential function is given on a set of grid points.

2.1.2. The Poisson Problem

The Poisson Problem is solved using a combination of the Newton-Raphson technique, Stoke's Theorem and the finite difference method. The Newton-Raphson technique is a method for root finding that may be used to define the potential Φ by rewriting the right hand side of the Poisson equation using a Taylor series expansion in $(\Phi - \Phi_0)$:

$$\rho(\Phi) = \rho(\Phi_0) + \rho'(\Phi_0)(\Phi - \Phi_0) + \frac{1}{2}\rho''(\Phi_0)(\Phi - \Phi_0)^2 \dots = 0.$$

If $(\Phi - \Phi_0)$ is small, the series can be truncated to its first couple of terms to give:

$$\rho(\Phi) = \rho(\Phi_0) + \frac{d\rho}{d\Phi} \Delta\Phi . \quad (2-26)$$

The densities that were calculated in the Vlasov Problem are the numerical values of eq.(2-26) for each grid point. The left hand side of eq.(1-1) can be defined using the finite difference method to discretize a partial differential equation and implement a numerical method, to produce the second order difference equation:

$$\frac{d^2\Phi}{dR^2} = \frac{(\Phi_{i+1} - 2\Phi_i + \Phi_{i-1}))}{\Delta R^2} . \quad (2-27)$$

The geometry of the problem is captured through Stoke's Theorem, which states:

$$\int_{Vol} (\nabla \times \vec{F}) \cdot d\vec{Vol} = \int_{Area} \vec{F} \cdot d\vec{Area} .$$

When $\Phi = \bar{F}$, Stoke's Theorem can be rearranged to give

$$\Phi = \frac{d^2\Phi}{dR^2} \frac{Vol}{Area} \Delta R.$$

When the Stoke's Theorem is applied to eq.(2-27), and the geometry terms are integrated into Poisson's equation, the result is:

$$\frac{\Phi_{i+1} - 2\Phi_i + \Phi_{i-1}}{\Delta R^2} = \frac{Vol}{Area} \Delta R 4\pi e (N_e - N_i).$$

In dimensionless terms, the above equation is:

$$\frac{\phi_{i+1} - 2\phi_i + \phi_{i-1}}{\Delta r^2} = \frac{Vol}{Area} \Delta r \frac{(n_e - n_i)}{\lambda_D^2}. \quad (2-28)$$

The solution to Vlasov's Problem gives $(n_e - n_i)$, defined as eq.(2-26); therefore, eq.(2-28) can be rearranged into a form that is equivalent to eq.(2-26):

$$\left\{ \left[\left(\frac{Area}{\Delta r} \right) \left(\frac{\lambda_D}{\Delta r} \right)^2 \left(\frac{1}{Vol} \right) \right] + \frac{d\rho}{d\Phi} \right\} (\phi_{i+1} - 2\phi_i + \phi_{i-1}) = -(n_e - n_i). \quad (2-29)$$

The negative value on the right hand side of eq.(2-29) accounts for the negative right hand side of Poisson's equation. From here, eq.(2-29) can be evaluated as a matrix and the potential ϕ can be solved for.

2.2. Turning Angle Calculations

It is more intuitive to express the equation of the orbit of a particle in terms of R and θ while eliminating the time dependence, with E and L as constants of integration. In a central force problem (where the only two forces interacting with each other are the particle and the probe), the orbit is symmetrical about the turning point, meaning that if

any two turning points are known, the complete orbit of the particle can be traced [Goldstein, 1980]. The classical equation of motion for angular momentum states that

$$L = mR^2\dot{\theta} \quad (2-30)$$

which can be rewritten as

$$d\theta = \frac{Ldt}{mR^2}. \quad (2-31)$$

Recognizing that $V_R = \frac{dR}{dt}$, the conservation of energy equation as defined as eq.(1-18)

can be rearranged to form a definition of dt :

$$dt = \frac{dR}{\sqrt{\frac{2}{m}\left(E - \Phi - \frac{L^2}{2mR^2}\right)}}. \quad (2-32)$$

Substituting $d\theta$ from eq.(2-31) into eq.(2-32) will eliminate t and provide a solution for the orbit in terms of θ , R and the constants of motion, given $\Phi(R)$:

$$d\theta = \frac{LdR}{mR^2 \sqrt{\frac{2}{m}\left(E - \Phi(R) - \frac{L^2}{2mR^2}\right)}}. \quad (2-33)$$

When eq.(2-33) is transformed into dimensionless units, and substituting in the turning function $g(r)$ as defined in eq.(1-27), the result is

$$d\theta = \frac{dr}{r \sqrt{\frac{g(r)}{J^2} - 1}} \quad (2-34)$$

In the case when $\phi(r) = \frac{\phi_p}{r}$, such as a sphere in a vacuum, an analytical answer

for $d\theta$ can be calculated. The equation is

$$d\theta = -\arccos \left(\frac{\frac{2J^2}{r\phi_p} - 1}{\sqrt{1 + \frac{4EJ^2}{\phi_p^2}}} \right). \quad (2-35)$$

By definition, the TPM identifies the position at which a particle of a certain energy and angular momentum will turn in a potential field. Viewed in (J^2, r) space as in Figure 2.2, a particle with an angular momentum of J^2 (held constant throughout the particle's orbit) will turn at a radius r when it intersects with the turning function (below the curve), g , and proceed back out to infinity along a trajectory symmetrical to its incoming path. $d\theta$ must be calculated numerically because analytic solutions such as eq.(2-35) have been found for only a small number of cases that have simple potential forms, and our general numerical solution for $\Phi(R)$ will obviously be unsuitable for analytic integration. Therefore, we can calculate the turning angle of a particle by computing the $d\theta$'s at each grid point out to infinity (effectively the end of the grid) and adding them together to form one θ value for each g function value. θ is interpreted according to the geometry illustrated in Figure 2.3 for attracted and repelled particles:

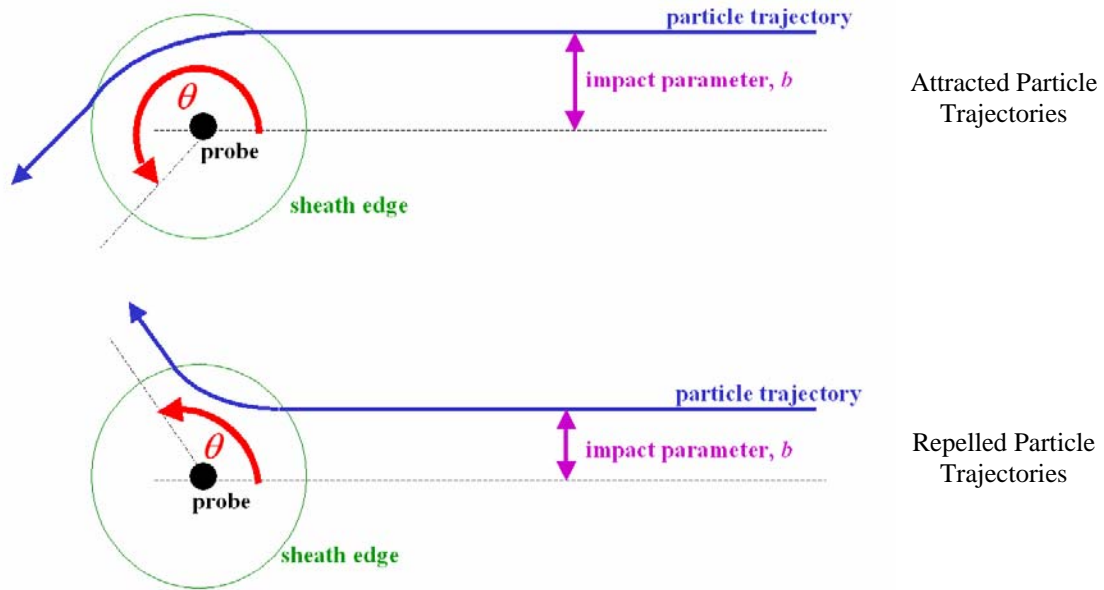


Figure 2.3: Attracted and Repelled Particle Trajectories

By examination of Figure 2.3 it is clear that for an attracted particle trajectory, the turning angle θ will approach 360° as the impact parameter b decreases, and approach 180° as the impact parameter reaches infinity. The repelled particle trajectories do the opposite – θ approach 0° as b decreases and converges to 180° as b goes to infinity.

2.3. Computational Implementation of the Turning Point Method

2.3.1. Solution of the Vlasov and Poisson Problems

Obtaining a numerical solution for the particle density, current density and electrical potential of a plasma requires simultaneously solving Vlasov's and Poisson's equations

through the solution of two sub-problems, the Vlasov Problem and the Poisson Problem. One fairly simple way to solve the two sub-problems is using an iterative procedure, consisting of developing radial grid points extending from the surface of the probe to an approximation of infinity. At each grid point, the Vlasov Problem is solved to yield the particle density, while the Poisson Problem is solved at the same time to yield the electrical potential to produce mutually consistent solutions.

A program called “TurningPoint” was developed by Cooke [1981] that simultaneously solved both problems using the TPM for a spherical probe. The program structure is outlined below.

- 1) Default values are set for all of the variables in the program.
- 2) User values are inputted into the program.
- 3) The velocity and mass grids are created, extending out from the probe surface to a specified end radius, usually to a distance where the potential goes effectively to zero; the grid cannot have more than 200 nodes (a program constraint), but it can extend as far as desired. More grid nodes translates into better electric potential resolution. The mass nodes are the cell centers, and share their index with the velocity node to the left.
- 4) Specific values, based in the inputted user values, are defined to be used in the program, including dimensionless values.
- 5) The boundary conditions are defined and the initial potentials are (usually) set to zero.
- 6) The potential matrix (Poisson’s equation $\nabla^2\Phi$) is built using the initial values.
- 7) The TPM is used to find the number and current density for ambient and local electrons and ions, essentially solving the Vlasov Problem.

7a) The g array is calculated and the min's and max's found (J_1^2 and J_2^2).

7b) The monoenergetic energies, M_n and M_i , are calculated using J_1^2 and J_2^2 .

7c) Current and number densities for the particles are calculated using the monoenergetic energies and integrating over the semi-infinite energy range using seven (or six) different energies derived from Laframbois and Stauffer [AAIA Journal, 1969].

7d) The calculated densities are used as the right hand side of Poisson's equation in order to calculate the potentials (up to this point the potentials were assumed).

8) The potentials for the particles are calculated by solving the potential matrices (a linear system of equations) using Gaussian elimination, effectively solving the Poisson Problem.

8a) Gaussian elimination is a method for solving the linear system of equations $A \times X = B$, where A is a tri-diagonal matrix and X and B are column vectors whose lengths are the total number of grid points used. Results are returned in X , while A is preserved and the contents of B are destroyed.

8b) In the TurningPoint program, B is the right hand side of eq.(2-29), X is the potential ϕ that we want to solve for, and A is a $[3 \times (\# \text{ of grid points})]$ matrix, consisting of all of the terms on the left hand side of eq.(2-29) other than ϕ . The matrix form of eq.(2-29) as it is evaluated in TurningPoint is as follows:

$$\begin{bmatrix} \text{cleft} \\ -(\text{cleft} + \text{cright}) - \frac{d\rho}{d\phi} \\ \text{cright} \end{bmatrix} \times \begin{bmatrix} \phi_{i-1} \\ \phi_i \\ \phi_{i+1} \end{bmatrix} = (n_e - n_i)$$

where $\lambda_d = \frac{\lambda_D}{dr}$, $\text{cleft} = \lambda_d^2 \frac{\text{Area}_{i-1}}{(r_i - r_{i-1}) \text{Vol}_{i-1}}$, and $\text{cright} = \lambda_d^2 \frac{\text{Area}_{i+1}}{(r_{i+1} - r_i) \text{Vol}_{i+1}}$

[Cooke, 1981].

9) The old potentials (the potentials calculated in the previous loop) are mixed using a Picard mixing technique with the potentials calculated in step 8) to get a new, more stabilized potential.

10) The grid is advanced one node and the new potentials become the old potentials for the next iteration.

11) Steps 7) through 10) are repeated for each grid node.

12) The trajectory of the particle is calculated for a given particle energy (the steps for this will be explained in the next section).

13) For a floating potential, the boundary conditions are defined again and steps 5) through 12) are repeated.

A graphical representation of the program flow is shown in Figure 2.4.

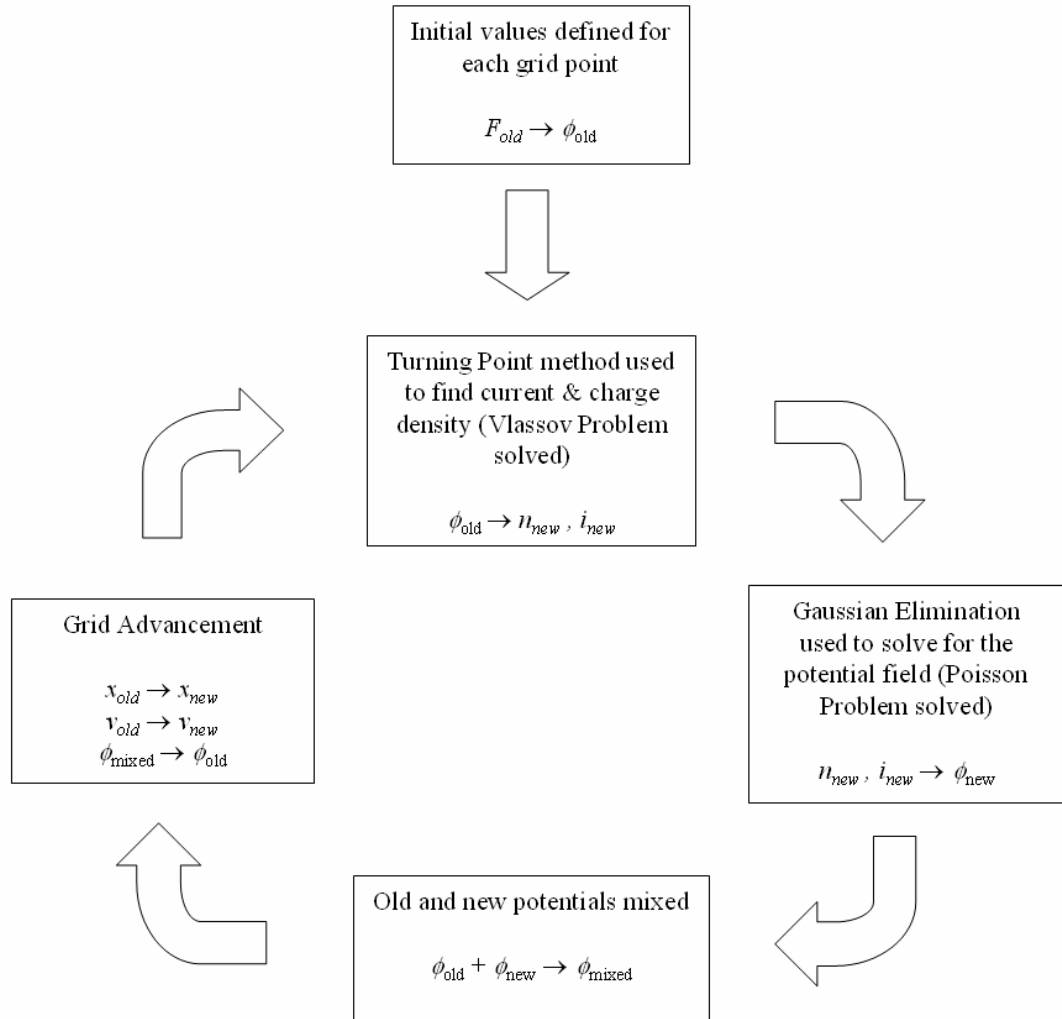


Figure 2.4: Graphical Representation of the TurningPoint Program Flow

For this thesis, the TurningPoint program that was developed by Cooke [1981] was expanded to include plasma analysis using a cylindrical probe as well as a spherical probe. The program modifications consisted of adding “IF” statements that, when the definition of “cylindrical” was initialized in the user inputs, the program would skip past the spherical definitions of the number and current density and their monoenergetic

contributions (equations (2-5), (2-15), (2-19) and (2-21)) and use the corresponding equations for the cylindrical solution (equations (2-6), (2-16), (2-20) and (2-22)).

2.3.2. Turning Angle Computations

The TurningPoint program by Cooke [1981] was also expanded to calculate the trajectory of a charged particle around either an attracting or repelling probe of cylindrical or spherical geometry by calculating the turning angle of the particle from its turning point out to the end of the grid, or an approximation of infinity. A separate subroutine, called “turn_angle”, was added to the end of TurningPoint that numerically calculates the turning angle of the particle at each grid point using the electric potential field of the probe defined earlier in the TurningPoint program. The steps in the subroutine are outlined below.

1) A new g array is calculated using the previously calculated potentials and a new, user-defined particle energy.

2) Minimums and maximums are identified in the g array in order to exclude particles that don't contribute to the angle calculation (only type-2 particles are considered).

3) One value of $d\theta$ is calculated for each impact parameter (or each g array value at each

grid point, given that $b = \sqrt{\frac{J^2}{E}}$ when $g = J^2$) according to the classical $d\theta$ eq.(2-34).

3a) The program starts at one g array value and calculates $d\theta$ for that specific point, when $g = J^2$ results in an inverse square singularity in the calculation of $d\theta$, using the

subroutine *midsql*. *Midsql* is a subroutine taken directly from Press [et.al., 1986] that solves the integral by using Romberg integration of an improper integral, specifically

$$\int_A^B f(x)dx = \int_0^{\sqrt{B-A}} 2tf(A-t^2)dt \quad , \quad B > A$$

for a singularity at A.

Nothing is known about the potential profile between the grid points; consequently, in order to integrate the $d\theta$ equation between each grid point the potential profile must be assumed for the g array term in eq.(2-34), as defined by eq.(1-27). For a spherical probe, the electric field in a vacuum varies as $E\alpha \frac{1}{r^2}$; for a cylindrical probe in a vacuum, $E\alpha \frac{1}{r}$. Since $E = \nabla\Phi$, the potential for a spherical probe varies as $\Phi = \frac{1}{r}$ for a small space charge, and $\Phi = \log(r)$ for large space charge. For a cylindrical probe, the potential varies as $\Phi = \log(r)$ for a small space charge and $\Phi = \frac{1}{r}$ for large space charge (see Figure 3.1).

3b) The rest of the integral is calculated using Simpson's extended rule, which states

$$\int_{x_1}^{x_N} f(x)dx = h\left[\frac{17}{48}f_1 + \frac{59}{48}f_2 + \frac{43}{48}f_3 + \frac{49}{48}f_4 + f_5 + f_6\right. \\ \left. \dots + f_{N-4} + \frac{49}{48}f_{N-3} + \frac{43}{48}f_{N-2} + \frac{59}{48}f_{N-1} + \frac{17}{48}f_N\right].$$

3c) The sum of the first integral, using *midsql*, and the sum of the rest of the integrals, using Simpson's extended rule, are added up to return a single theta value.

4) Step 3) is repeated for every value of the g array to produce an array of turning angles specific to the particle's energy.

3. Results and Validation

3.1. Cylindrical Probe Sheath Approximations

Several runs of TurningPoint were performed using different Debye lengths and probe voltages to obtain a potential distribution and approximate a sheath radius for the case of a cylindrical probe. Most runs were done with a Debye length that was within the OML limit (i.e. a Debye length that is equal to or greater than the probe radius). The expected result is that as the space charge decreases (as the Debye length gets larger) and the probe voltage decreases, the sheath radius will decrease, and vice versa. The potential distributions of several TurningPoint runs are shown in Figure 3.1.

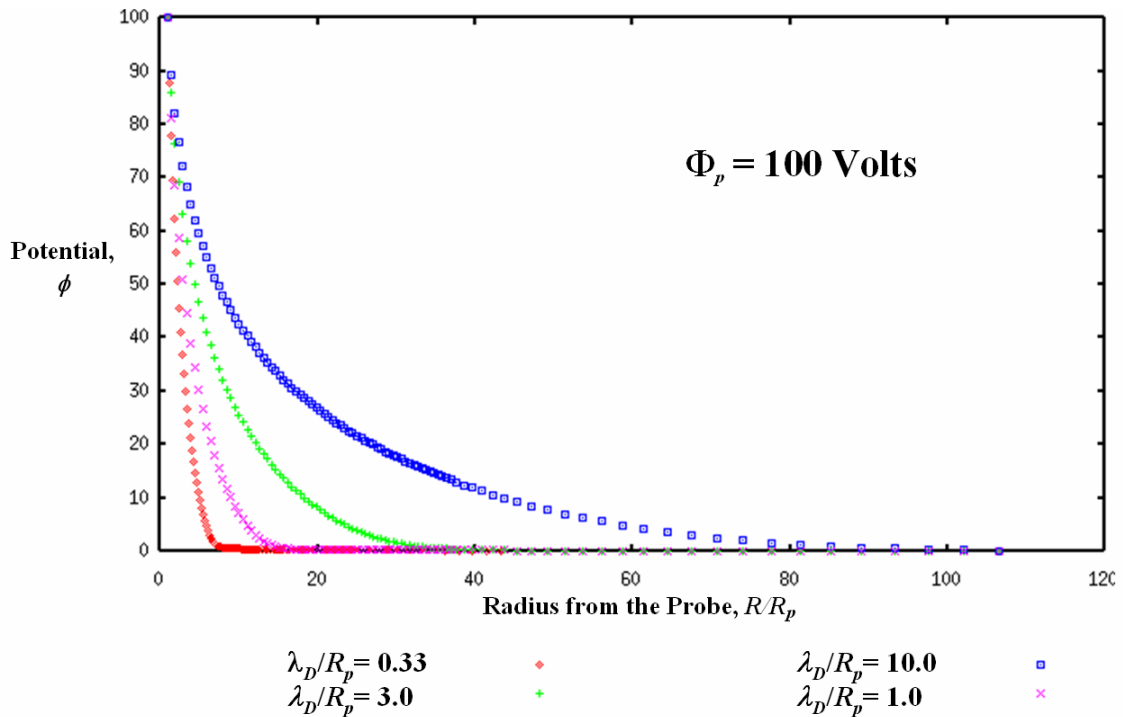


Figure 3.1: Electric Potential vs Radius from the Probe For Different Debye Lengths

Figure 3.1 also shows the expected result that at large space charge (low $\frac{\lambda_D}{R_p}$), the potential profile approaches a $\frac{1}{r}$ characteristic, while at a small space charge (high $\frac{\lambda_D}{R_p}$) the potential profile approaches a $\log(r)$ characteristic. At the sheath edge where the electric field of the probe is weak, the thermal energy of the attracting species (kT) will have just enough energy to escape from the potential well and not contribute to the collected probe current; it is therefore approximated that the sheath is located at a radius from the probe where the particle thermal energy is equal to the potential energy of the plasma inside the sheath, or when $\frac{\Phi}{kT} \cong 1.0$. The sheath radius for different potential distributions and Debye lengths can then be approximated, as shown in Figure 3.2:

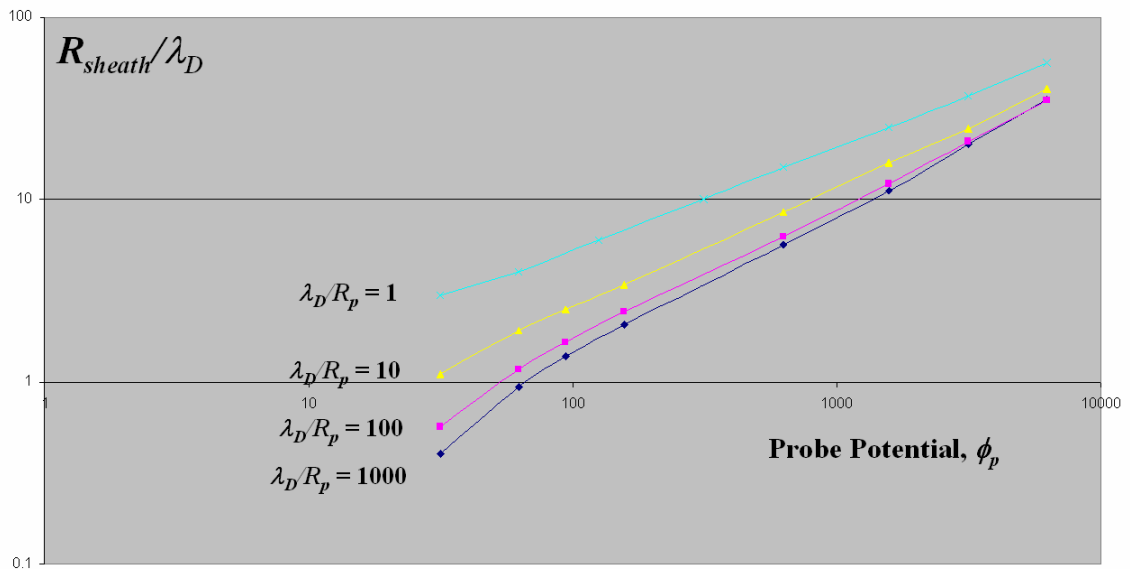


Figure 3.2: Sheath Radius vs Probe Potential

It is possible to extrapolate a relationship between the sheath radius and the probe potential by recognizing that the sheath radius plotted against the probe potential in a log-log plot as in Figure 3.2 follows the relation

$$\frac{R_{sheath}}{\lambda_D} \approx \phi_p^x \rightarrow \ln\left(\frac{R_{sheath}}{\lambda_D}\right) = x \ln(\phi_p).$$

The result is that $\frac{R_{sheath}}{\lambda_D} \propto \phi_p^{0.75}$, consistent with Choiniere's work [Choiniere, 2004].

The results from TurningPoint were also validated by comparing Laframboise's earlier work [Laframboise, 1966] with the TurningPoint results for current collection in the OML limit. Figure 3.3 is the dimensionless current versus the dimensionless probe potential for a cylindrical probe from Laframboise.

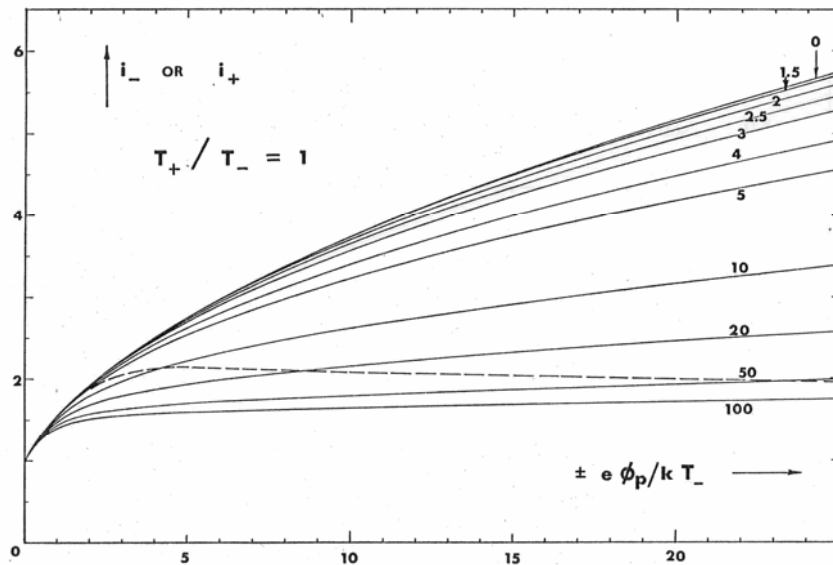


FIGURE 39 ION OR ELECTRON CURRENT VS PROBE POTENTIAL FOR VARIOUS RATIOS OF PROBE RADIUS TO ION OR ELECTRON DEBYE LENGTH; CYLINDRICAL PROBE; $T_+/T_- = 1$. DOTTED CURVE SHOWS TRAPPED-ORBIT BOUNDARY.

Figure 3.3: Probe Current i vs Probe Potential ϕ_p for a Cylindrical Probe [Laframboise, 1966]

The results from TurningPoint are consistent with Laframboise, as shown in Table 3.1.

R_p/λ_D	Current, i
1	5.17
3	4.73
10	3.10
20	2.39

Table 3.1: Results from TurningPoint, $\phi_p = 20$

3.2. Turning Angle Approximations

Several particle trajectories were defined for different amounts of space charge for both attracting and repelling particles in a cylindrical and spherical probe sheath. For a probe voltage held at +100 Volts, the turning angle for various attracted and repelled particles of ± 100 Volts for varying amounts of space charge are shown in Figure 3.4.

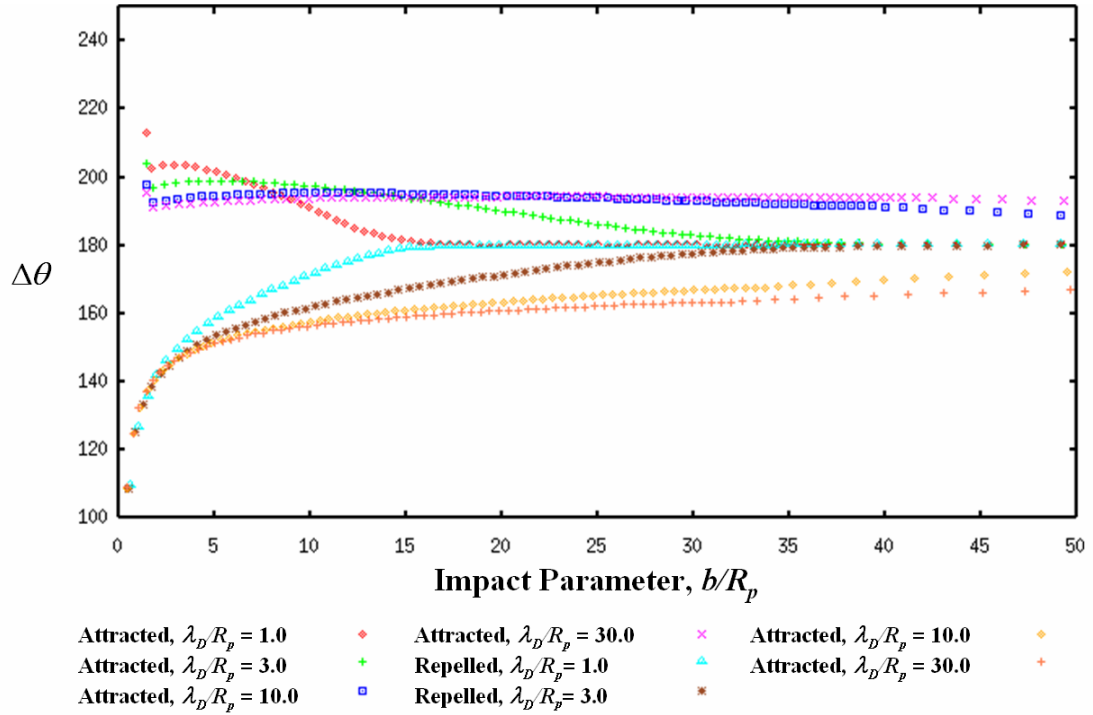


Figure 3.4: Turning Angle vs Impact Parameter for Attracted and Repelled Particles where $\Phi_p = +100$ Volts and $\Phi_{particle} = \pm 100$ Volts

As expected, Figure 3.4 shows the repelled particles coming towards the probe from infinity, where their turning angle is 180° , and being increasingly repelled from the probe as they approach. At a close enough impact parameter, the particles are repelled completely and cannot reach the probe. Figure 3.5 illustrates that a +10 Volt particle approaching a +100 Volt probe cannot even penetrate the probe sheath until it reaches an impact parameter of $\sim 4 \times R_p$, with a turning radius of $\sim 27 \times R_p$.

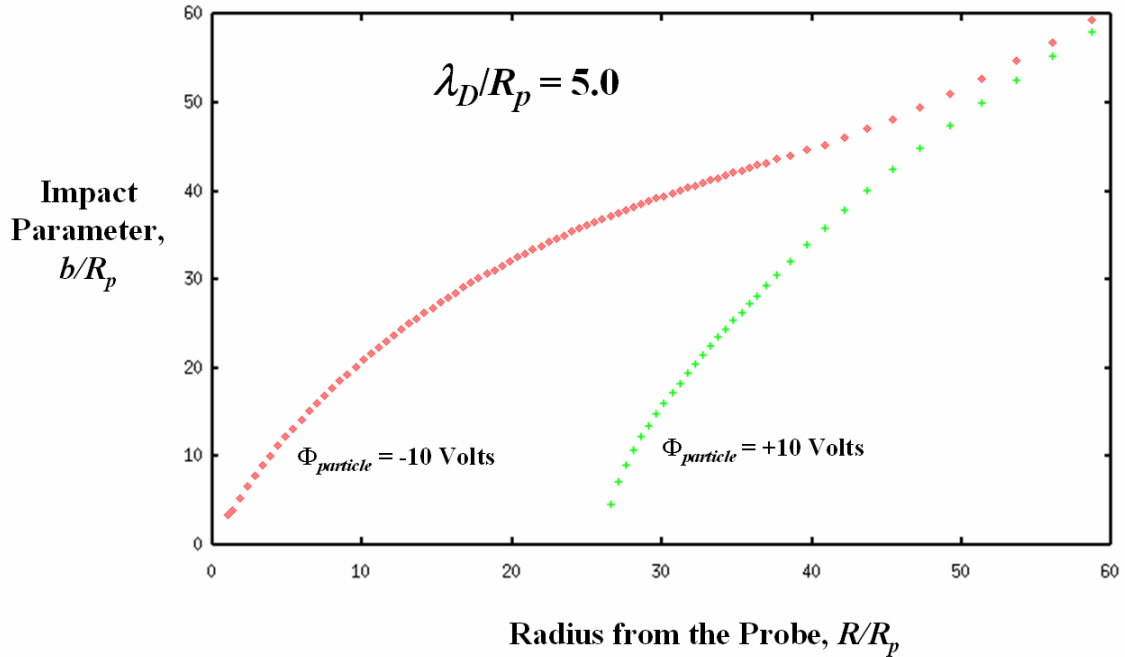


Figure 3.5: Radius from the Probe vs Impact Parameter for $\Phi_p = +100$ Volts and $\Phi_{particle} = \pm 10$ Volts

An attracted particle coming into the probe from infinity will fall into the probe and approach 360° . Figures 3.4 and 3.6 illustrate an interesting phenomenon as the particle first enters the probe sheath – the deflection angle initially jumps up, suggesting that the particle gains $\Delta\theta$ as it transverses across the contours of the probe sheath and then slopes down as the impact parameter decreases and the particle avoids the sheath irregularities. The effect is more striking as the space charge of the plasma increases and the probe sheath radius decreases.

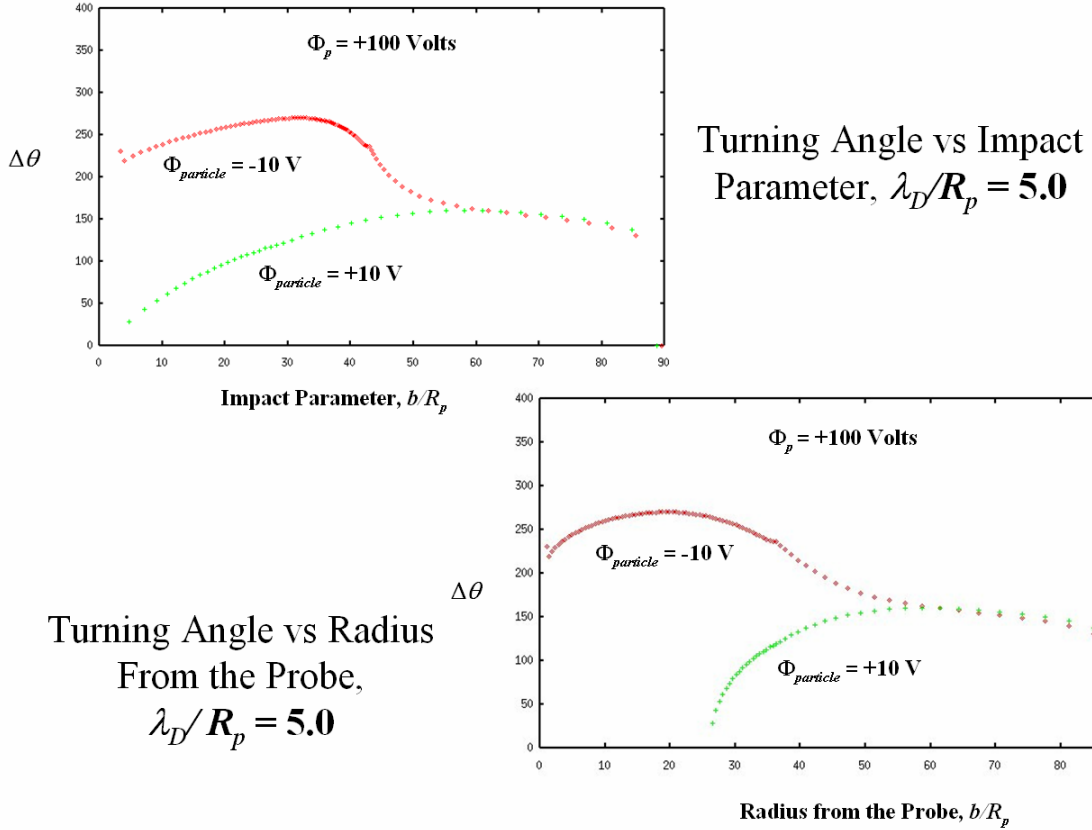


Figure 3.6: Turning Angle vs Radius from the Probe and Impact Parameter

The behavior of the potential profile as shown in Figure 3.1 makes it possible to test for consistency of the numerical results by comparing the analytical solution for $\Delta\theta$, eq.(2-35), with the TurningPoint results when the potential profile is forced to be $\phi(r) = \frac{\phi_p}{r}$. The results, shown in Figure 3.7, illustrates what the turning angle of a particle of varying energies in a plasma of high space charge would be in the absence of a sheath. The results from TurningPoint and Goldstein [1980] correlate very well with each other, validating the turn_angle subroutine. It is of interest to note that, even though this

probe analysis dealt with space charges within the OML limit, significant changes in orbital trajectories between different space charges were still observed.

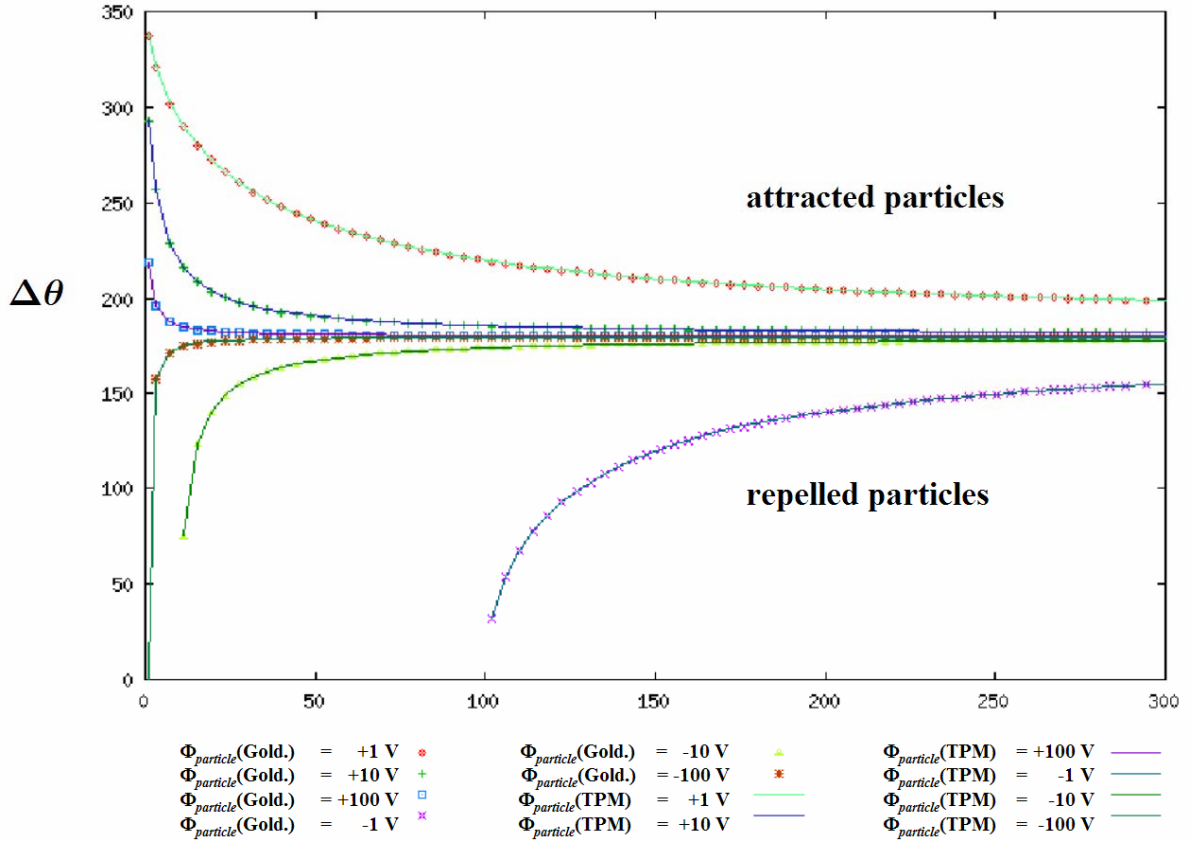


Figure 3.7: Turning Angle vs Impact Parameter for Attracted and Repelled Particles for the Case When $\phi(r) = \frac{\phi_p}{r}$, $\Phi_p = +100$ Volts. $\Phi_{particle}(\text{Gold.})$ refers to results obtained using eq.(2-35), and $\Phi_{particle}(\text{TPM})$ refers to results obtained using the TurningPoint program.

Result so far support the common sense expectation that higher plasma shielding (low $\frac{\lambda_D}{R_p}$) limits the range of impact parameters that experience significant scattering.

Because the analysis of orbital trajectories does not yield information about the intensity of the incoming particles, a discussion about the total scattering cross-section of the particles is not possible. However, the first moment of the orbital trajectories can be

calculated, as $\theta_{moment} = \langle \theta \rangle \times r_{sheath}$, providing a somewhat arbitrary number that reflects the quantity of particles that will be deflected to some degree by the probe. Table 3.2 illustrates the result that higher plasma shielding limits the range of impact parameters that

λ_D/R_p	Attracted, θ_{mom} (radians x R/R_p)	Repelled, θ_{mom} (radians x R/R_p)
1	35.6	40.6
3	144.4	159.9
5	264.6	294.3
10	431.1	510.0
30	571.2	708.5

experience significant scattering.

Table 3.2: Turning Moment, $\Phi_p = 100$ Volts

4. Summary and Recommendations for Future Work

4.1. Summary of Work and Conclusions

The purpose of this thesis was to manifest the Turning Point Method (TPM), developed by Parker, into a computer program that models plasma interactions with charged probes of spherical and cylindrical geometries. The original program, developed by Cooke, was designed only as a spherical probe model and was expanded to include cylindrical geometries and particle trajectory calculations. The one-dimensional case assumes an infinite wire in an unmagnetized plasma with finite and equal ion and electron temperatures. Because particle energy and angular momentum are conserved in such a formulation, the results have the potential to provide a standard against which to compare more complicated simulations.

The cylindrical probe model was successfully integrated into the original TurningPoint program. The sheath radius and the probe potential for different space charges were plotted on a log-log plot in order to determine the relationship between them, with the result being $\frac{R_{sheath}}{\lambda_D} \propto \phi_p^{0.75}$. The analytically extrapolated relationship is consistent with Choiniere's earlier work with the KiPS program [Choiniere, 2004]. Results are also validated by comparing Laframboise's earlier work [Laframboise, 1966] with the TurningPoint results for current collection in the OML limit. The dimensionless current versus the dimensionless probe potential for a cylindrical probe as calculated in

the TurningPoint program are consistent with Laframboise's graphical results of the same characteristics.

Calculations of the turning angle of a charged particle with specific energy and angular momentum revealed that higher plasma shielding limits the range of impact parameters that experience significant scattering, and that attracted particles entering tangent to the sheath experience increased scattering. Several particle trajectories were defined for different levels of space charge for both attracting and repelling particles in a cylindrical and spherical probe sheath. Attracted particles coming into the probe from infinity will fall into the probe and approach a turning angle of 360° , while repelled particles will approach 0° as their impact parameter decreases, eventually becoming unable to penetrate the sheath at all. The deflection angle of the particle also temporarily jumps up when the particle travels across the contours of the sheath. The results also show that there are significant changes in orbital trajectories between different space charges within the OML limit.

4.2. Recommendations for Future Work

1. Additional subroutine into the turn_angle program that will generate a 2-D graph of the trajectory of the particle around the probe. This would include writing the $d\theta$ values for each impact parameter (step 3 of the turn_angle subroutine) into a separate file and plotting each file using the Unix plotting program gnuplot. By doing this, the trajectory of each specific particle can be tracked and an illustration of the particle's interaction with the probe can be made.

2. Modification the `turn_angle` program so that it uses the `midsql` subroutine for the entire $d\theta$ integral, eliminating the need for Simpson's extended rule. The Romberg integration that `midsql` uses is more accurate than Simpson's extended rule because Simpson's extended rule assumes equal step sizes throughout the integration, while the Romberg integration used in `midsql` calculates the exact step size between each grid point (dr) and uses that value in its calculations. The spatial grid used in the main program `TurningPoint` is designed to be able to expand and contract according to the programmer's discretion, so the step sizes are often not equal throughout the entire grid. The unequal step sizes result in increased error when using Simpson's extended rule, especially when the grid is programmed to expand rapidly past the sheath boundary, which is often the case since the potential drops off rapidly at this distance and detailed information about this region is not critical.

3. Change the integration method used to solve eq. (2-35) for the first interval, where `midsql` is used (steps 3a)) from a method where the potential profile of the sheath region is assumed ($\frac{1}{r}$ for high space charge, $\log(r)$ for low space charge) to a method that extrapolates the potential profile as the calculation proceeds. The turning angle calculation can be treated as an initial value problem, where the values and derivatives of the variables are known at some starting point but not known at some end point (in this case, the potentials at each grid point are known, but the potentials between the grid points are not known). The second order differential equation that defines the potential

profile, which is Poisson's equation, can be rewritten as two first order differential equations, and those first order differential equations can be reduced down to a set of algebraic formulas that "step" through the function, achieving a good approximation of the differential equation when the step size is very small. The literal implementation of this is Euler's method, which states

$$y_{n+1} = y_n + hf'(x_n, y_n).$$

However, Euler's method on its own is not ideal for practical use due to its inaccuracy compared to other methods run at equivalent step sizes and its instability [et.al., 1986]. A better method is the fourth-order Runge-Kutta method, as described in Press [Press et.al., 1986], which propagates a solution of the potential profile over an interval by combining the information from four Euler-style steps and using that information to match a Taylor series expansion up to the fourth order.

The Runge-Kutta method can be integrated into the `turn_angle` program by using the subroutine "`RK4`", taken directly from Press [et.al., 1986], and calling it when the `g` array is calculated for use in eq.(2-34). As `midsql` loops through each step in the integration between two grid points, it will also loop through the `RK4` subroutine and solve for the potential at each step.

4. Compare the results of the TurningPoint program to other more complicated programs.

References

Bernstien, I.B. and Rabinowitz, I.N., "Theory of Electrostatic Probes in a Low-Density Plasma", The Physics of Fluids, Vol.2, Mar. 1959.

Birdsall, C.K. and Langdon, A.B., Plasma Physics Via Computer Simulation, McGraw-Hill Inc., New York NY, 1985.

Chen, Francis F., Introduction to Plasma Physics, Plenum Press, New York NY, 1974.

Choiniere, E., "Theory and Experimental Evaluation of a Consistent Steady-State Kinetic Model For 2D Conductive Structures In Ionospheric Plasmas With Application To Bare Electrodynamic Tethers In Space", Briefing at the University of Michigan, Ann Arbor, May 2004.

Cooke, D.L., "A Self-Consistent Computer Model for the Solar Power Satellite-Plasma Interaction", Rice University, Houston TX, May 1981.

Dendy, R.O., Plasma Dynamics, Oxford University Press, NY, 1990.

Goldstein, H., Classical Mechanics, 2nd Ed., Addison-Wesley, MA, 1980.

Hutchinson, I.H., "Principles of Plasma Diagnostics," Cambridge University Press, 1987.

Hoyt, R.P. and Minor, B.M., “Remediation of Radiation Belts Using Electrostatic Tether Structures”, IEEEAC Paper #2.0801, 2005.

Laframboise, J.G., “Theory of Spherical and Cylindrical Langmuir Probes in a Collisionless Maxwellian Plasma at Rest”, University of Toronto Institute of Aerospace Studies, Rept.100, June 1966.

Laframboise, J.G. and Parker, L.W., “Probe Design for Orbit-Limited Current Collection”, The Physics of Fluids, Vol.16, No.5, May 1973.

Langmuir, I. and Mott-Smith, H.M., “The Theory of Collectors in Gaseous Discharges”, Physics Review, Vol.28, 1926.

Lieberman, Michael A. and Lichtenberg, Allan J., Principles of Plasma Discharges and Materials Processing, John Wiley & Sons Inc., New York NY, 1994.

Parker, L.W., and Whipple, E.C., Jr., “Theory of a Satellite Electrostatic Probe”, Annals of Physics, Vol.44, Aug.1967.

Parker, L.W., “Computer Solutions in Electrostatic Probe Theory”, Mt.Auburn Research Associates, Inc., Newton MA, AFAL-TR-72-222, Apr. 1973.

Parker, L.W., “Theory of Electron Emission Effects in Symmetric Probe and Spacecraft Sheaths”, Lee W. Parker, Inc., Concord MA, AFGL-TR-76-0294, Sept.1976.

Parker, L.W., “Plasma-Photosheath Theory for Large High-Voltage Space Structures”, Space Structures and Their Interactions With Earth’s Space Environment, Vol.71, AIAA 1980.

Press, W.H., Flannery, B.P., Teukolsky, S.A., and Vetterling, W.T., Numerical Recipes: The Art of Scientific Computing, Cambridge University Press, New York NY, 1986.

Roussel, J.F., “NASCAP Features: A Brief Review of NASCAP Code (series) Features”, http://195.101.59.123/ls-web/spine/spine/meeting/spineM4/docs/slides/Roussel_NASCAP.pdf, 2005.

Soop, M., “Numerical Calculations of the Perturbation of an Electric Field Around a Spacecraft”, Photon and Particle Interactions with Surfaces in Space, edited by R.J.L.Gard, D. Reidel, Hingham MA, 1973.

Steen, N.M., Byrne, G.D., and Gelbard, E.M., “Guassian Quadratures for the Integrals $\int_0^{\infty} \exp(-x^2)f(x)dx$ and $\int_0^b \exp(-x^2)f(x)dx$ ”, Mathematics of Computation, Vol.23, 1969.

Tethers Unlimited, Inc. Science Ops, “About Space Tethers”,
<http://www.tethers.com/TethersGeneral.html>, 1994-2004.

Tidman, Derek A., Shock Waves in Collisionless Plasmas, Wiley-Interscience, NY,
1971.